Biomechanics of Myocardial Ischemia and Infarction

Colleen M. Witzenburg and Jeffrey W. Holmes

Abstract Each year, over seven million people suffer a myocardial infarction (heart attack). For those who survive the initial event, the mechanical properties of the scar tissue that gradually replaces the damaged muscle are a critical determinant of many life-threatening sequelae, such as infarct rupture and the development of heart failure. Thus, understanding the mechanics of healing infarct scar, its interaction with the rest of the heart, and the resulting changes in heart function are critical to devising effective therapies. Computational models play an essential role in understanding these potentially complex interactions. The first section of this chapter reviews the structure and mechanical properties of the normal heart and the methods used to study those properties. The second section discusses the structure and mechanical properties of healing post-infarction scar. The remaining sections review landmark analytical and computational models that provided insight into the functional consequences of myocardial infarction and potential therapies. Finally, we briefly consider emerging models of wound healing in the infarct region and growth and remodeling in the surviving myocardium that are beginning to predict the long-term effects of infarction and post-infarction therapies. In the future, multi-scale models that capture such remodeling in addition to the beat-to-beat mechanics of the heart hold great promise for designing novel therapies, not only for myocardial infarction but also for a wide range of cardiac pathologies.

1 Structure and Mechanical Properties of Myocardium

In order to assess changes in myocardial structure, mechanics, and function that result from ischemia and infarction, it is important to first understand the mechanics of the normal heart. Thus, this section reviews the basic anatomy and mechanical properties of heart tissue (myocardium), with an emphasis on the experimental testing methods used to determine myocardial mechanical properties.

C.M. Witzenburg · J.W. Holmes (✉)
University of Virginia, Charlottesville, VA, USA
e-mail: holmes@virginia.edu

G.A. Holzapfel and R.W. Ogden (eds.), *Biomechanics: Trends in Modeling and Simulation*, Studies in Mechanobiology, Tissue Engineering and Biomaterials 20, DOI 10.1007/978-3-319-41475-1_6

1.1 Anatomy and Structure of the Heart

The heart is a muscular pump that circulates blood throughout the body. It is comprised of four chambers and four valves. Deoxygenated blood returning from the body through the veins first reaches the right atrium; it then flows through the tricuspid valve into the right ventricle, and is pumped through the pulmonary valve to the lungs. Oxygenated blood leaving the lungs enters the left atrium, flows across the mitral valve into the left ventricle (LV), and is pumped through the aortic valve into the network of arteries that carry blood throughout the body (West 1985).

The size and shape of the four heart chambers vary considerably, as does the pressure they typically generate during contraction. The atria are irregularly shaped with walls that are just 1–2 mm thick; normal atria experience peak pressures of roughly 10 mmHg (a little more than 1 kPa). By contrast, in adult humans the LV is shaped like a truncated ellipsoid with 10 mm thick walls and generates pressures exceeding 100 mmHg during contraction. The right ventricle is crescent-shaped in cross section, wrapping partially around the LV, with which it shares a common wall called the interventricular septum. The normal human right ventricular (RV) free wall is 3–4 mm thick. Pressures in the RV are roughly 1/5 those of the LV (West 1985).

The muscle cells (myocytes) in the heart are arranged end-to-end and coupled tightly to one another both electrically and mechanically. Although individual myocytes frequently branch and connect to two other myocytes rather than one, on gross inspection or in low-magnification micrographs of any small region of the left and right ventricles there is a clear preferred fiber orientation. Over the years, many anatomists and physiologists have studied the muscle fiber structure of the LV and sought to understand how this structure relates to heart mechanics and function; a compilation of drawings from several influential studies is reproduced in Fig. 1 from a review by Buckberg et al. (2008).

One central feature of the left ventricular muscle fiber structure is that the fiber orientation changes through the depth of the wall. Near the outer surface of the heart (epicardium), muscle fibers are oriented approximately 60° clockwise from the circumferential direction, while near the inner surface (endocardium), they are oriented approximately 60° counterclockwise from the circumferential direction (Fig. 1). One functional consequence of this arrangement is that as the heart contracts and relaxes, it also twists. Among early studies of heart structure, the work of Streeter and colleagues exerted a particularly strong influence on subsequent computational models, because these investigators carefully quantified both left ventricular shape and fiber orientation, and fitted these data with continuous functions that are straightforward to incorporate into analytical and finite element models of the heart (Streeter and Hanna 1973a, b).

In addition to the muscle fibers, connective tissue surrounding and linking the myocytes makes an important contribution to the mechanical properties of the heart (Fomovsky et al. 2010). Histologic sections taken parallel to the muscle fibers show large collagen fibers running parallel to the myocytes. These collagen fibers comprise

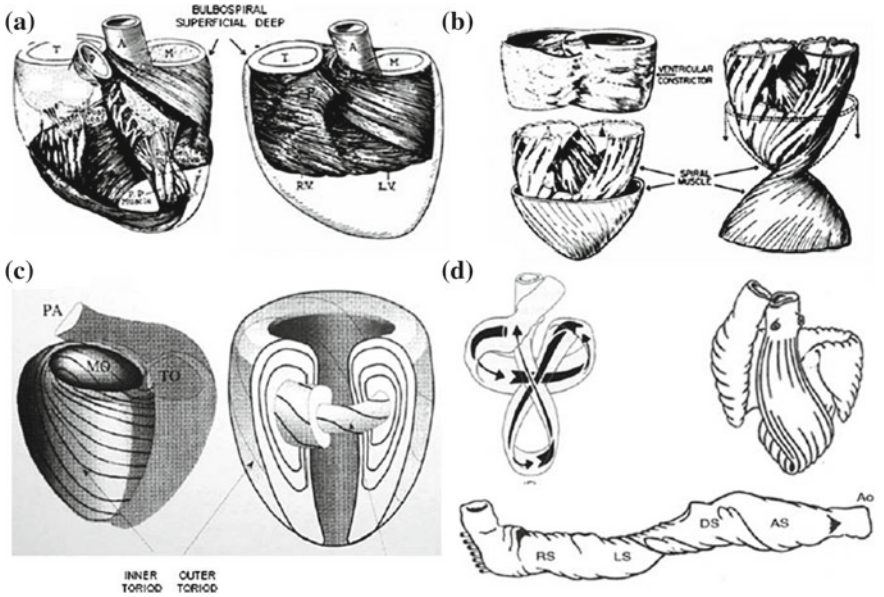

Fig. 1 Drawings from several classic studies of left ventricular fiber structure, reproduced from Buckberg et al. (2008): **a** McCallum (1900); **b** Rushmer et al. (1953); **c** Streeter (1979); **d** Torrent-Guasp (1967). These drawings illustrate the oblique angles of muscle fibers in the inner and outer layers of the heart wall, and the difference in fiber orientations between these layers

2–3 % of the tissue volume in normal hearts, and at low pressures they appear wavy or coiled whereas at high pressures they appear flat and unfolded. Therefore, at very low pressures or stresses these fibers likely contribute little to the mechanical properties of the heart, but as the heart is inflated to higher pressures and the collagen fibers straighten, they gradually bear more of the load (Fomovsky et al. 2010). For the passively inflated LV, this arrangement results in an exponential pressure-volume curve that becomes quite steep at high pressures. In addition to these large collagen fibers, histologic studies show layers of connective tissue that separate muscle fibers into parallel sheets approximately 4–5 myocytes thick (LeGrice et al. 2001), as well as small collagen struts that connect the myocytes and sheets to one another (Caulfield and Borg 1979). Recent experimental and modeling studies suggest that this laminar organization is an important determinant of left ventricular mechanics (Costa et al. 1999; Usyk et al. 2000). However, the overall contribution of extracellular matrix to heart mechanics remains an active and important area of investigation. Furthermore, while it is generally recognized that collagen and myocyte structure in other chambers—particularly the atria—differ from those in the LV (Ho et al. 2002; Zhao et al. 2012), much work remains to define these structures and incorporate them into models.

Muscle fibers and the surrounding extracellular matrix are arguably the most important determinants of the mechanical properties of myocardium, but there are

other important contributors that are not discussed in detail here. For example, a network of coronary blood vessels supplies blood to the heart and interacts dynamically with the surrounding myocardium. Compression of coronary vessels by the myocardium limits blood flow during systole (Lee and Smith 2012), while pressurization of the coronary tree alters the compliance of the heart (May-Newman et al. 1994). Many of the mechanical testing methods described below start by excising tissue, disconnecting it from its blood supply; obviously, such tests cannot capture the contributions of coronary blood flow to heart mechanics.

1.2 Mechanical Testing of Myocardium

The material properties that govern the response of normal and diseased tissues to mechanical loading are centrally important in the field of biomechanics. However, in the case of the heart, determining those material properties by appropriate testing is complicated by the geometry and architecture outlined above. Pressures in the individual chambers of the heart and deformation within its walls can be measured directly in an intact heart, but the corresponding stresses must be estimated using analytical or computational models and cannot be directly verified. Alternatively, pieces of myocardium can be excised and tested ex vivo; however, in practice cutting injury and contracture of the myocytes typically complicate such experiments. Consequently, experimentally determining the properties of fully relaxed, passive myocardium using the methods reviewed below has proven quite challenging. Yet understanding the passive response is only a beginning, as myocardial material properties vary throughout the cardiac cycle due to the cyclic contraction and relaxation of the individual myocytes.

1.2.1 Passive Inflation of Arrested Hearts

One of the most straightforward preparations for assessing heart mechanics is the isolated heart. Typically, the heart is perfused with a cold, oxygenated cardioplegia solution to block contraction while preserving cell viability. The heart is then excised along with a portion of the aorta, which is mounted onto a cannula. Fluid flowing into this cannula from the aorta toward the heart (retrograde perfusion) forces the leaflets of the aortic valve closed and flows into the coronary arteries through their ostia in the aortic root, providing control over myocardial temperature, oxygenation, and chemical environment. Often, a balloon is introduced into the left ventricular cavity to provide control over left ventricular volume, while a pressure transducer integrated in the balloon provides real-time pressure data.

Suga and Sagawa (1974) used a version of this isolated heart preparation to explore the pressure-volume behavior of the actively contracting heart. They perfused the coronary arteries of isolated hearts with warm, oxygenated blood and stimulated the hearts electrically to induce contraction at a regular rate. One of their simplest

experiments was to hold volume in the balloon constant during an entire contraction and measure the maximum pressure the heart could generate under specified conditions. Other studies included using a computer-controlled servopump to vary balloon volume over time in order to simulate the filling, emptying, and isovolumetric phases of a normal cardiac cycle. Many other physiologists have used similar approaches—particularly a version called the Langendorff preparation—to study aspects of heart physiology ranging from electrical activation to contraction to metabolism (Bell et al. 2011).

McCulloch et al. (1987) employed isolated, arrested canine hearts to study the passive material properties of myocardium. In addition to inserting a balloon into the left ventricular cavity, they placed a triangle of sutures on the epicardial surface and tracked the motion of these markers using video during inflation of the intracavitary balloon to simulate diastolic filling. Using the images of the markers, they computed regional strains on the epicardial surface during inflation. They found that principal strains during inflation differed substantially in magnitude, that the direction of principal epicardial stretch was close to the fiber direction, and that the LV twists as it inflates. These data suggested that passive myocardium was mechanically anisotropic and provided important validation data for emerging models of LV mechanics.

The major advantages of the isolated heart preparation for characterizing left ventricular mechanics are that: (i) the heart remains intact with its coronaries perfused; (ii) the boundary conditions—pressure applied to the inner wall of the LV and deformation constrained only at the mitral valve ring—are reasonably physiologic; (iii) the myocardium can be activated for study of time-varying material properties. The major disadvantages are that: (i) stresses in the LV wall cannot be measured directly; (ii) the range of stresses that can be applied along the different material axes (e.g., parallel vs. transverse to the fibers) is limited by the geometry of the heart.

1.2.2 Planar Biaxial Testing

Circumferential and longitudinal stresses in the wall of the inflated LV are tensile, while radial stresses are compressive on the endocardium and zero (or very small if the pericardium is intact) at the epicardial surface. Therefore, another common approach to determine the passive material properties of myocardium is biaxial testing in the circumferential-longitudinal plane (Fig. 2). Much of the early work in this area was done by Yin and colleagues (Demer and Yin 1983; Yin et al. 1987). They prepared samples for testing by slicing the LV wall into sheets 1–2 mm thick, and mounted them so that the test axes were aligned with the predominant fiber and crossfiber directions. Then, they subjected the myocardial samples to many combinations of stretch in the fiber and crossfiber directions while measuring the net forces imposed along each test axis. They found that passive myocardium was nonlinear, viscoelastic, and anisotropic, having greater stiffness along the fiber direction (Demer and Yin 1983). Furthermore, the two directions were mechanically coupled: stress in each

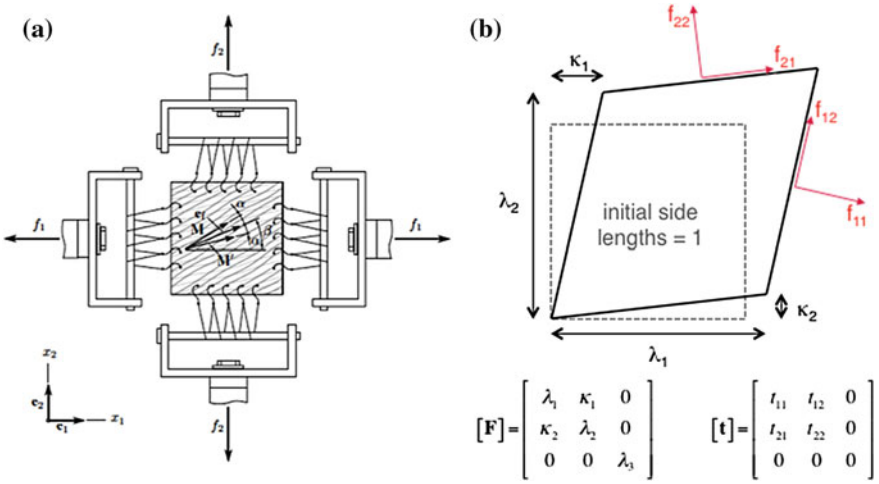

Fig. 2 Kinematics of planar biaxial testing of myocardium: **a** Schematic of typical test setup, showing force transducers that measure a single force in each test direction, reproduced by permission from Sommer et al. (2015). **b** Assuming a state of plane stress, in general there are five nonzero components of the deformation gradient **F** and three independent, nonzero components of the Cauchy stress matrix ($t_{12} = t_{21}$, see text) related to the four force components f_{ij} applied to the sample edges. Computing three nonzero stresses from two net forces requires making additional assumptions (Fomovsky and Holmes 2010; Sommer et al. 2015)

test direction depended on stretch in both directions (Demer and Yin 1983; Yin et al. 1987).

One of the best biaxial testing studies on myocardium was published by Humphrey et al. (1990a, b). Following an approach suggested by Rivlin and Saunders (1951) for isotropic materials, Humphrey et al. (1990a, b) postulated a transversely isotropic strain-energy function for myocardium that depended on two invariants of the right Cauchy–Green tensor. They imposed combinations of stretches that held one invariant constant while changing the other. Then, they used the measured stresses and stretches to estimate the derivatives of the strain-energy function with respect to those invariants. Plotting the derivatives against the invariants allowed them to determine the form of the polynomial strain-energy function that best fit their experimental data. This elegant approach takes advantage of a major advantage of biaxial testing: it provides excellent control over the loading protocol, allowing application of any desired combination of fiber/crossfiber stretch or load. Other important advantages include the ability to align the test axes with the anatomic fiber and crossfiber directions, and the ability to directly compute stresses from experimentally measured forces. The major disadvantages of planar biaxial testing for characterizing the passive material properties of myocardium are the need for extensive dissection and the related difficulty of preventing contracture of the sample.

One important warning regarding biaxial testing is that in practice, the computation of stresses is not always straightforward. As shown in Fig. 2, if samples are thin

enough relative to their other dimensions so that plane stress is a reasonable assumption, only three independent components of the Cauchy stress matrix are nonzero (the Cauchy stress matrix is symmetric, $t_{12} = t_{21}$, per conservation of angular momentum). When the fiber axis is aligned with one of the test axes, there is little or no shear deformation, and the force components f_{12} and f_{21} and shear stresses $t_{12} = t_{21}$ vanish. Such biaxial tests are useful in identifying material parameters that affect resistance to stretch in the fiber or crossfiber direction, but do not provide information on the shear behavior of the myocardium. In theory, it should be possible to obtain additional information on shear behavior by intentionally orienting the fiber direction oblique to the test axes, but in practice most testing devices are not designed to separately measure the normal (f_{11} and f_{22}) and lateral (f_{12} and f_{21}) force components applied to the sample edges. Rather, most investigators introduce additional assumptions that may affect the accuracy of the computed stresses (Fomovsky and Holmes 2010; Sommer et al. 2015).

An increasingly popular approach is to map deformation across biaxial samples using large numbers of markers, and combine test data with sample-specific finite element models to extract material parameters. A major advantage of this approach is that it allows for more realistic variations in material properties across a sample. However, conceptually such approaches are more like model-based extraction of properties from isolated heart experiments—the results depend on the choice of the underlying constitutive model, and predict spatial variations in stress that are difficult to verify.

1.2.3 Extension and Torsion of Papillary Muscles

Humphrey et al. (1992) proposed an alternate approach to biaxial mechanical testing of myocardium that requires less dissection and is therefore less influenced by cutting injury. Taking advantage of prior theoretical work on torsion and extension of cylinders, they developed an analytical solution for the stresses in the central region of a papillary muscle induced by first stretching, then twisting the muscle. Papillary muscles connect the left (or right) ventricular walls to the mitral (or tricuspid) valves and surrounding valve rings. Dissecting them free requires cutting into myocardium at one end (where they connect to the wall) and severing the chordae tendinae at the other end (where they connect to the valve and surrounding valve ring). The resulting sample is relatively long and thin, with muscle fibers aligned parallel to its long axis. Although this process does induce some damage at one end, the damage appears to have little effect on behavior in the central region of the muscle. Accordingly, early cardiac physiologists often used papillary muscles for studies of basic cardiac muscle physiology.

During uniaxial extension of a papillary muscle, relating the applied axial load to measured axial stretch is straightforward and provides information about material properties along the muscle fiber axis. Humphrey et al. (1992) realized that by twisting the papillary muscle at different axial extensions and relating the applied moment to measured shear strains, they could also obtain information on shear properties.

Thus, they could experimentally determine coefficients for a transversely isotropic constitutive law that depended only on the first invariant of the right Cauchy–Green tensor and on the stretch in the fiber (axial) direction. Advantages of this approach include: (i) ease of dissection; (ii) excellent control over the loading protocol; (iii) known orientation of the test axes relative to the anatomic fiber and crossfiber directions; (iv) the ability to directly compute stresses from the measured axial force and moment. The primary disadvantages of this approach relate to the anatomic differences between papillary muscles and the myocardium within the ventricular walls that may limit use of information obtained from papillary muscles: (i) papillary muscles are enclosed in a fibrous sheath that may contribute significantly to the measured mechanics (Criscione et al. 1999); (ii) papillary muscles do not contain the laminar sheet structure identified elsewhere in the heart wall. Thus, although a transversely isotropic constitutive model may be appropriate for papillary muscles, the resulting parameters do not capture the orthotropic nature of the myocardium in the heart walls. One other potential benefit of papillary muscle testing is the ability to study active in addition to passive properties. The most important caveat with such studies is that the metabolic demands of cardiac muscle are quite high, even at rest; therefore, diffusion from a surrounding fluid bath is often insufficient to supply papillary muscles with adequate oxygen (Holmes et al. 2002). Testing the thinner right ventricular papillary muscles or even very small trabeculae dissected from the inner surface of the heart wall can help avoid confounding effects from hypoxia at the center of the muscles.

1.2.4 Shear Testing

Dokos et al. (2002) developed one final approach to material testing of passive myocardium designed to more fully characterize properties of the myocardium within and across the laminar sheets (LeGrice et al. 1995, 2001). They cut myocardium into cubes with the edges aligned with the local fiber, sheet (perpendicular to the fibers within the sheets), and sheet-normal (perpendicular to the sheet surfaces) directions. They then glued the top and bottom of each cube to parallel metal plates and sheared them while measuring both the shear and axial forces applied by their device. By applying shear in different directions to different faces of the cubes, these investigators were able to quantify the response to a much wider range of deformations than would be possible with any of the other tests discussed above, and clearly relate those tests to the anatomic structure of the tissue. Relative to the other methods discussed here, the obvious disadvantage of testing small cubes of myocardium is that it requires much more dissection.

1.3 Mathematical Descriptions of Myocardial Properties

Any mathematical description of passive myocardium must account for both its anisotropic nature and its nonlinear behavior. The most common approach is to

formulate a strain-energy function, a potential function with the property that its derivatives with respect to strains or stretches yield expressions for the components of the stress tensor. Polynomial, exponential, or pole-zero formulations for the strain-energy function are the most frequently used in cardiac mechanics. Some of these equations contain a large number of material coefficients; however, the testing methods described above allow the unique identification of only a handful of coefficients.

As described above, Humphrey et al. (1990a, b) used biaxial test data both to determine the functional form of a polynomial strain-energy function and to identify the material parameters in that formulation. They assumed myocardium was pseudoelastic, incompressible, transversely isotropic, and locally homogenous, and that the stress was a function of only the first, I_1, and the fourth, I_4, invariants of the right Cauchy–Green tensor $\mathbf{C}$. Their strain-energy function contained five material constants:

$$W = c_1(\sqrt{I_4} - 1)^2 + c_2(\sqrt{I_4} - 1)^3 + c_3(I_1 - 3) + c_4(I_1 - 3)(\sqrt{I_4} - 1) + c_5(I_1 - 3)^2. \quad (1)$$

In a subsequent study, Novak et al. (1994) used the same strain-energy function to quantify transmural mechanical differences across the heart wall and found that the orientation of the preferred direction changes through the wall, and that myocardium is stiffer near the endocardium and epicardium than at the midwall.

Guccione et al. (1991) employed a Fung-type exponential form in their finite element simulations of inflation, extension, and torsion of a thick-walled cylinder representing the passive canine LV:

$$W = \frac{C}{2}\exp\left[2b_1(E_{RR} + E_{FF} + E_{CC}) + b_2 {E_{FF}}^2 + b_3({E_{CC}}^2 + {E_{RR}}^2 + {E_{CR}}^2 + {E_{RC}}^2) + b_4({E_{RF}}^2 + {E_{FR}}^2 + {E_{FC}}^2 + {E_{CF}}^2)\right] - \frac{C}{2}, \quad (2)$$

where C, b_1, b_2, b_3, and b_4 are material constants, $\mathbf{E}$ is the Green–Lagrange strain tensor, and the subscripts R, F, C refer to the radial, fiber, and crossfiber directions, respectively. They also treated the myocardium as pseudoelastic, transversely isotropic, and incompressible, and obtained best-fit values for the coefficients by minimizing the error between model-predicted epicardial strains and those reported by McCulloch et al. (1989) during passive inflation of isolated, arrested hearts. Based on the work of LeGrice et al. (1995, 2001) and Dokos et al. (2002) discussed in Sect. 1.2, Costa et al. (2001) extended the strain-energy function employed by Guccione et al. (1991) to model the myocardium as orthotropic rather than transversely isotropic.

Holzapfel and Ogden (2009) proposed an alternate exponential strain-energy function that accounts for the orthotropy of myocardium, and fitted their function to both the biaxial testing data of Yin et al. (1987) and the shear data of Dokos et al. (2002):

$$W = \frac{a}{2b}\{\exp[b(I_1 - 3)] - 1\} + \frac{a_F}{2b_F}\{\exp[b_F(I_{4F} - 1)^2] - 1\} + \frac{a_S}{2b_S}\{\exp[b_S(I_{4S} - 1)^2] - 1\} + \frac{a_{FS}}{2b_{FS}}\{\exp[b_{FS}{I_{8FS}}^2] - 1\}, \quad (3)$$

where I_1 is the first invariant, I_{4F} is the fourth invariant associated with the fiber direction, I_{4S} is the fourth invariant associated with the sheet direction, and I_{8FS} is a coupling invariant involving both the sheet and fiber directions.

One other approach in the literature is the pole-zero formulation. Again treating myocardium as orthotropic and incompressible and guided by experimental results showing an extremely steep rise in stress approaching a limiting strain in each direction, the group at the University of Auckland developed a strain-energy function of the form

$$W = \frac{k_{FF}{E_{FF}}^2}{|a_{FF} - E_{FF}|^{b_{FF}}} + \frac{k_{NN}{E_{NN}}^2}{|a_{NN} - E_{NN}|^{b_{NN}}} + \frac{k_{SS}{E_{SS}}^2}{|a_{SS} - E_{SS}|^{b_{SS}}} + \frac{k_{FN}{E_{FN}}^2}{|a_{FN} - E_{FN}|^{b_{FN}}} + \frac{k_{FS}{E_{FS}}^2}{|a_{FS} - E_{FS}|^{b_{FS}}} + \frac{k_{NS}{E_{NS}}^2}{|a_{NS} - E_{NS}|^{b_{NS}}}, \quad (4)$$

where the subscripts N, F, S refer to the normal, fiber and sheet directions (Nash and Hunter 2001). This function contains 18 material constants, making it impractical to identify all the coefficients through direct mechanical testing. Accordingly, Nash and Hunter (2001) suggested that some of the parameters might be estimated from histological data.

Most studies simply select one of these formulations based on convenience, familiarity, or ease of numerical implementation. However, a few studies have compared various features of these strain-energy functions. Holzapfel and Ogden (2009) discussed the stability of these strain-energy functions and identified all of those listed here as convex and strongly elliptic except for the polynomial form of Humphrey et al. (1990a). Schmid et al. (2006, 2008) fitted the data of Dokos et al. (2002) both directly and using a finite element model. They compared several strain-energy functions including the pole-zero formulation and the orthotropic exponential formulation of Costa et al. (2001). They fitted each function to the test data and compared goodness of fit, between-specimen variability of the fitted parameters, and the numerical stability of the optimization process. Overall, Schmid et al. (2006, 2008) concluded that the exponential function of Costa et al. (2001) provided the best balance between fitting the data well with fewer parameters and limiting between-specimen variability in parameter values.

2 Structure and Mechanical Properties of Myocardial Scar Tissue

Following interruption of the normal blood supply to a region of the heart, the affected myocytes stop contracting within the first minute (Tennant and Wiggers 1935) and begin to die within the first hour (Connelly et al. 1982). Due to the prevalence of coronary artery disease in Western societies, occlusion of coronary arteries long enough to induce myocyte death—termed myocardial infarction (MI)—is common, with over 7 million new infarctions per year worldwide (White and Chew 2008). Most patients now survive the initial infarction, and many reach the hospital quickly enough to undergo procedures such as thrombolysis or balloon angioplasty to reopen the occluded arteries, limiting the total amount of damage. However, the myocytes that die during the infarction cannot regenerate; instead, dead myocytes are gradually resorbed and replaced by a collagenous scar. Over the weeks and months following MI, the evolving structure and mechanical properties of the healing infarct scar are an important determinant of heart function as well as of the likelihood of a range of serious post-infarction complications such as infarct rupture, infarct expansion, and heart failure (Holmes et al. 2005). Accordingly, understanding the mechanical properties of the evolving scar—and how those properties affect growth, remodeling, and function of the heart—is an important and active area of cardiovascular biomechanics research.

2.1 Myocardial Scar Structure

The cellular and extracellular composition of a healing myocardial infarct evolves rapidly over the first days and weeks following the initial injury. Initially, white blood cells invade the damaged region, secreting proteolytic enzymes and removing debris through phagocytosis. These inflammatory cells also secrete growth factors that encourage invasion and proliferation of fibroblasts, the cells that deposit the extracellular matrix proteins that make up the scar tissue. Extracellular matrix (ECM) deposition by fibroblasts increases rapidly after the first few days, and ECM protein content continues to increase for the next several weeks. Although the maturing scar contains many different collagens, proteoglycans, and other ECM proteins, collagen is thought to account for most of the mechanical properties of post-infarction scar tissue; accordingly, this section will focus on changes in collagen content and structure. Several recent review articles provide more detail on the pathology of infarct healing and changes in other ECM components (Lindsey and Zamilpa 2012; Frangogiannis 2014; Richardson et al. 2015).

2.1.1 Collagen Content and Crosslinking

Collagen content begins to rise 4–7 days after infarction and typically reaches a plateau by 3–6 weeks, depending on the animal model. Whereas collagen occupies about 3 % of the area of a histologic section of normal myocardium, reported collagen area fractions range from roughly 30 % in the rat (McCormick et al. 1994; Fomovsky and Holmes 2010) to 60 % in the pig (Holmes et al. 1997) and dog (Clarke et al. 2015) following permanent coronary ligation. An alternate approach to measuring collagen content is to measure the concentration of the modified amino acid hydroxyproline and then estimate the percentage of collagen by weight assuming that the weight of collagen is 7.42 the times the weight of hydroxyproline; this method gives slightly lower estimates of about 25 % collagen by weight in mature rat infarcts (McCormick et al. 1994; Fomovsky and Holmes 2010) and 45 % in dogs (Jugdutt and Amy 1986). In addition to collagen content, the degree of crosslinking of the collagen molecules can affect tissue mechanical properties. Studies of crosslinking during infarct healing suggest that crosslink density initially rises with a similar time course to collagen, but may continue to rise even after collagen content plateaus (Vivaldi et al. 1987; Zimmerman et al. 2001; Fomovsky and Holmes 2010).

2.1.2 Collagen Alignment

Another potentially important determinant of scar mechanics is collagen fiber alignment. In some tissues such as tendon and ligament, highly aligned collagen results in a mechanically anisotropic tissue that resists tension much more effectively along the fiber axis than transverse to it. Early studies of infarct healing focused on collagen content rather than alignment, but more recent studies have revealed that the collagen fiber structure of healing infarct scars varies dramatically across different animal models. One reason that many early studies missed this variation is that the collagen fibers in healing infarcts lie in planes parallel to the epicardial surface, but histologic sections are typically cut perpendicular to the epicardial surface, making collagen fiber orientation difficult to visualize. Histologic sections cut parallel to the epicardial surface reveal highly aligned fibers following permanent coronary ligation in dogs (Whittaker et al. 1989; Clarke et al. 2015) and pigs (Holmes and Covell 1996); in these infarcts, the collagen fibers in the midwall are strongly aligned in the circumferential direction, while at the epicardium and endocardium fibers are oriented obliquely and are less strongly aligned (Holmes et al. 1997; Clarke et al. 2015). By contrast, Fomovsky and Holmes (2010) showed that following coronary ligation in rats, collagen fibers are randomly oriented (Fig. 3), resulting in scars that are not only structurally but also mechanically isotropic.

In a subsequent study, Fomovsky et al. (2012b) used liquid-nitrogen-cooled probes to create cryoinfarcts (well-defined regions of cell death) with controlled sizes, shapes, and locations on the rat LV. They found that infarcts in different locations on the LV experienced different patterns of stretch, which correlated with the collagen fiber structure observed three weeks later: infarcts that stretched similarly in

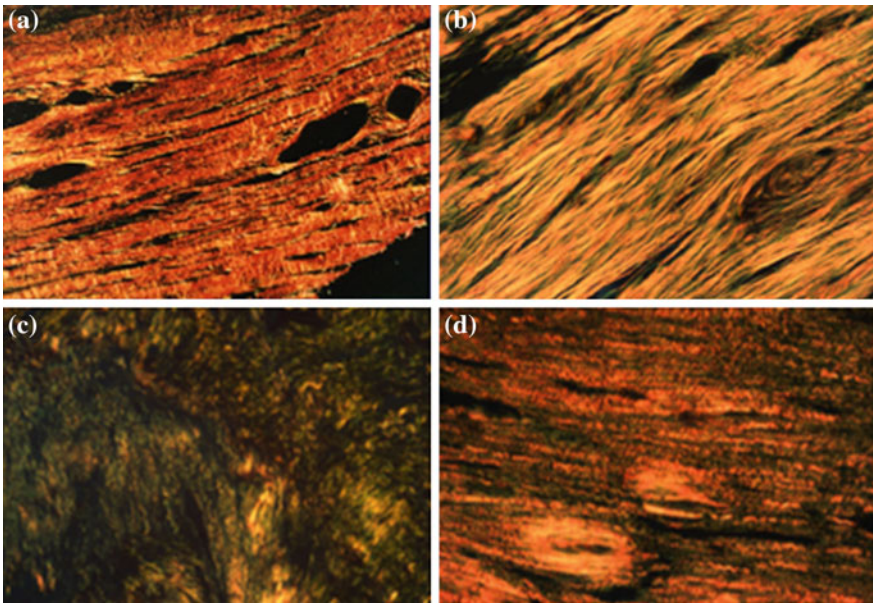

Fig. 3 Illustration of differences in collagen fiber alignment in histologic sections taken from the center of the infarct scar in different experimental models and imaged under polarized light: **a** pig, three weeks after ligation of a branch of the left circumflex (LCx) coronary artery (Holmes and Covell 1996); **b** dog, eight weeks after ligation of the left anterior descending (LAD) coronary artery (unpublished data from Clarke et al. 2015); **c** rat, three weeks after ligation of the LAD (unpublished data from Fomovsky and Holmes 2010); **d** rat, three weeks after cryoinfarction of the anterior wall at the mid-ventricle (unpublished data from Fomovsky et al. 2012b)

both the circumferential and longitudinal directions during healing formed scars with randomly oriented collagen fibers (similar to rat ligation infarcts), while those that stretched in only the circumferential direction contained circumferentially aligned collagen fibers (similar to pig ligation infarcts). Therefore, differences in mechanics during healing may explain the different collagen fiber structures reported in different animal models.

2.2 Myocardial Scar Mechanics

Within minutes after a region of the heart is deprived of blood flow, it stops contracting actively and begins to stretch and recoil passively as the stress in the heart wall rises and falls with each heartbeat. In some respects, the fact that the material properties of the healing scar vary little over the cardiac cycle makes studying infarct mechanics simpler than studying the mechanics of normal myocardium. However, because infarct composition, material properties, and volume all change as the scar forms and

remodels, comprehensive studies that measure infarct mechanics and composition at multiple time points are needed to understand not only the natural time course of healing but also the response of the heart to clinical post-infarction therapies. Given the clinical importance of myocardial infarction, surprisingly few such studies have been performed.

2.2.1 In Vivo Deformation

Some of the best early studies of infarct and scar mechanics used implanted measurement devices to track changes in local deformation over time. Tyberg et al. (1974) sutured strain gauges to the surface of the LV of dog hearts and plotted gauge length in the fiber direction against the pressure in the LV cavity. During normal contraction, these plots traced out counterclockwise loops very similar to the pressure-volume loops often employed to study cardiac physiology: segment length increased as the heart filled during diastole, remained nearly constant during isovolumetric contraction, decreased as the LV ejected blood into the aorta, and then remained nearly constant during isovolumetric relaxation (Fig. 4a). Following occlusion of the coronary artery supplying blood to the study region, the area inside the pressure-length loops rapidly decreased, reflecting the loss of active mechanical work by the muscle fibers; in some cases, the plots again traced out loops but in the opposite (clockwise) direction, suggesting that the ischemic segments were dissipating work done by the rest of the heart.

Tyberg et al. (1974) also reported an interesting shift in the end-diastolic dimensions of the regions they studied. They found that even when measured at an identical pressure at end diastole, segment lengths were significantly longer after 30 min of coronary occlusion. This finding was surprising, because it seems unlikely that the

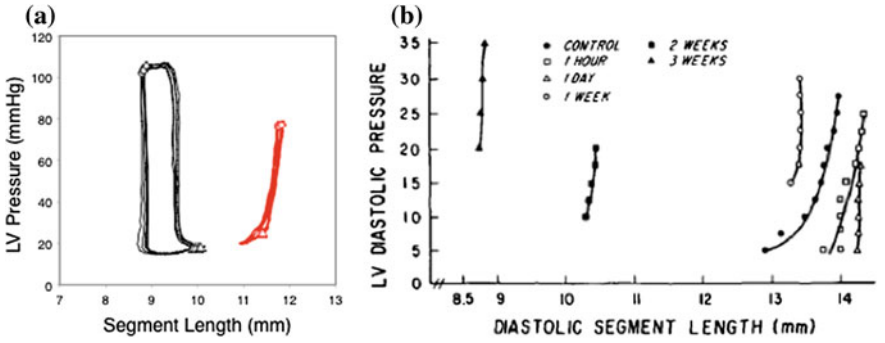

Fig. 4 **a** Pressure-circumferential segment length loops in an anesthetized dog at control (*black*) and 15 min after coronary ligation (*red*) show conversion from active shortening to passive stretching and recoil (data from the study of Fomovsky et al. 2012a). **b** Evolution of diastolic pressure-segment length curves in a healing canine infarct indicating substantial geometric remodeling of the healing scar (Theroux et al. 1977)

structure or composition of the ischemic region could change significantly in just 30 min. Some have postulated that a phenomenon called strain softening, observed in soft materials such as rubber, could play a role. However, Holmes et al. (2005) proposed a simpler alternative explanation that highlights the potential limitations of using in situ measurements to deduce information about material properties in the heart: occluding a coronary artery decreases blood flow, tissue volume, and wall thickness in the affected region of the heart. Holmes et al. (2005) estimated that this decrease in wall thickness due to loss of perfusion could increase stresses enough to explain the observation of Tyberg et al. (1974) of increased diastolic stretch at matched pressure.

Around the same time that Tyberg et al. (1974) performed their study of acute ischemia, Theroux et al. (1977) published a series of studies on longer term changes in regional segment lengths during healing of myocardial infarcts in dogs. This group used implanted sonomicrometers to measure segment lengths at multiple time points in the same animals. They reported that end-diastolic lengths increased slightly ($3 \pm 2\,\%$) immediately after injury (consistent with the study of Tyberg et al. 1974), remained elevated for about a week, but then decreased as much as 30 % by week 4 (Fig. 4b). A number of subsequent studies confirmed that infarcts can shrink in volume significantly as scar forms (Richardson et al. 2015), an important consideration when predicting the long-term effects of post-infarction therapies (Clarke et al. 2015).

Because the diastolic portion of their pressure-length curves had an exponential shape, Theroux et al. (1977) plotted lengths measured during filling (x-axis) against the natural log of the corresponding pressures (y-axis) in each dog at each time point and compared the slope of those curves as an index of regional stiffness. They found that the slope increased nearly 10 fold in the first day, then remained nearly constant over the next four weeks. However, as discussed in Sect. 1.2.1, the slopes of such curves depend not only on the changing passive material properties of the study region but also on the pressure and the geometry of the LV, which determine where the material is operating along its nonlinear stress–strain curve. Accordingly, ex vivo mechanical testing has provided the best information to date on changes in infarct material properties during healing, as reviewed in the next section.

Since these early studies, many groups have used implanted markers, sonomicrometers, ultrasound, and MRI to examine patterns of deformation in healing infarcts. Three broad themes emerge from these studies. First, in most animal models of permanent ligation of a coronary, strains drop to near zero in the infarct region and remain small throughout healing (Theroux et al. 1977; Holmes et al. 1994; Fomovsky and Holmes 2010). In studies with the resolution to distinguish these small strains statistically from zero, the circumferential and longitudinal strains are typically positive (indicating stretching of the scar during systole) and the radial strain is negative (indicating wall thinning in the infarct region). Unlike in the myocardium, where there are large variations in strain magnitude across the heart wall, in transmural infarcts the strains change little with depth (Villareal et al. 1991). The second broad trend is that when the occluded coronary artery is reopened before all of the downstream myocardium dies ('reperfused' infarcts), circumferential and longitudinal shortening often recover partially (Theroux et al. 1977; Kramer et al. 1997; Bogaert et al. 1999;

Kidambi et al. 2013). Finally, the third trend is that coupling to adjacent surviving myocardium can induce unexpected shears or other deformations in the infarct region that are tricky to interpret. For example, Holmes et al. (1994) measured large radial thickening strains in dense collagenous scars 3 weeks after infarction in pigs; although such strains normally indicate wall thickening due to active contraction, no surviving myocytes were apparent on histology in these scars.

One final point deserves mention regarding the interpretation of in vivo strains in healing infarcts. The convention in most cardiac mechanics studies is to compute deformation between end diastole, when muscle fibers in the heart wall are usually at their maximum length, and end systole, when they are at their minimum length. However, circumferential and longitudinal segment lengths in a passively deforming infarct typically reach their minimum length at the end of isovolumetric relaxation, when LV pressure is minimum, and their maximum at the end of isovolumetric contraction, when wall stress is greatest (Richardson et al. 2015). Therefore, infarct mechanics studies that compute strains from measurements taken only at end diastole and end systole likely neglect a substantial portion of the deformation.

2.2.2 Ex Vivo Mechanical Testing

Two of the approaches reviewed in Sect. 1.2 have also been employed for ex vivo testing of myocardial scar tissue: passive inflation of isolated arrested hearts and planar biaxial testing. Holmes et al. (1997) inflated isolated, arrested pig hearts three weeks following coronary ligation while tracking three-dimensional deformation in both the infarct scar and the remote myocardium. Consistent with the highly anisotropic collagen fiber structure shown in Fig. 3a, these scars stretched by as much as 40 % in the longitudinal direction but less than 15 % in the circumferential direction at a cavity pressure of 25 mmHg; by comparison, peak strains in the remote myocardium were approximately 30 % (longitudinal) and 35 % (circumferential) at the same cavity pressure. By contrast, Omens et al. (1997) measured epicardial strains during passive inflation of isolated arrested rat hearts 2 weeks after coronary ligation and reported greater infarct stretch in the circumferential direction than in the longitudinal direction. However, Fujimoto et al. (2007) reported equal circumferential and longitudinal infarct strains in passively inflated rat hearts 8 weeks after MI. Unfortunately, as discussed in Sect. 1.2.1, comparing infarct material properties across these studies would require constructing computational models to estimate circumferential and longitudinal wall stresses at each pressure.

To date, only two comprehensive biaxial testing studies have quantified the mechanics of healing myocardial scar tissue over time, and these studies reached very different conclusions. Gupta et al. (1994) studied anteroapical infarcts induced by coronary ligation in sheep. They reported average circumferential and longitudinal stresses at 15 % equibiaxial extension at 4 h, 1w, 2w, and 6w, and found that infarct anisotropy varied with time: longitudinal stresses were significantly higher at 1 week, while circumferential stresses were higher at six weeks. They also found that stresses in both directions peaked at 1–2 weeks and then decreased by six weeks, which was

unexpected given that they also reported a progressive increase in collagen content with time. By contrast, Morita et al. (2011) observed isotropic stretch under equibiaxial stress 8 weeks after MI in the same animal model. Fomovsky and Holmes (2010) conducted biaxial testing of rat anteroapical infarcts induced by coronary ligation and found that scars were mechanically isotropic at 1w, 2w, 3w, and 6w. Furthermore, the fitted material coefficient in their isotropic strain-energy function increased with time post-infarction, and correlated reasonably well with collagen content on a sample-by-sample basis. While the fact that different animal models develop post-infarction scars with different degrees of structural anisotropy (see Sect. 2.1.2) may explain differences in the levels of mechanical anisotropy reported by Gupta et al. (1994) and Fomovsky and Holmes (2010), it is more difficult to explain why collagen content and material properties were correlated in Fomovsky's study (Fomovsky and Holmes 2010) but decoupled in Gupta's (Gupta et al. 1994).

3 Analytical Models of Heart Function During Ischemia and Infarction

The primary function of the heart is to pump blood through the body. Therefore, the ultimate goal of studying the biomechanics of the normal and diseased heart is to understand the underlying basis for the heart's ability to perform this function, and how disease impairs pump function. Due to the complex geometry of the heart, measuring changes in tissue properties is usually necessary but not sufficient to quantitatively predict changes in overall pump function; researchers also typically employ a geometric or computational model to relate pressures and volumes inside the chambers of the heart to the stress and strain experienced by the myocardium that comprises those chambers. One of the most surprising things about the heart is that despite the complexity of its anatomy, geometry, and material properties, very simple analytical models can provide critical insight regarding heart function even in the setting of a myocardial infarction.

3.1 Normal Pump Function of the Left Ventricle

One of the most useful conceptual frameworks for analyzing pump function of the heart from an engineering perspective is the pressure-volume loop (Fig. 5). The idea of plotting volume against pressure to analyze the performance of a pump or engine is familiar to most engineers who have taken a course in thermodynamics. Pioneering physiologists such as Otto Frank applied this same idea to the heart over a century ago, plotting the internal pressure and volume of the LV against one another; in the 1970s and 1980s, Kiichi Sagawa and his colleagues at Johns Hopkins University

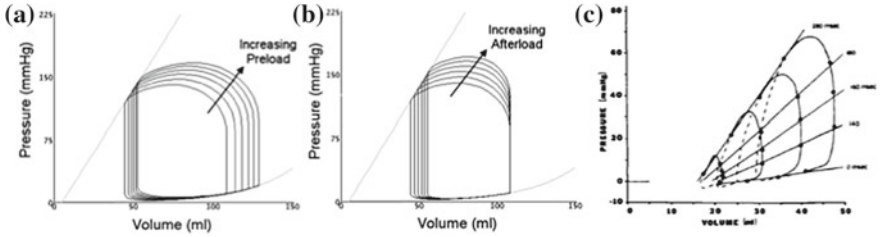

Fig. 5 **a** Simulated response of the isolated left ventricle to changes in filling pressure (preload) or, **b**, resistance to ejection (afterload). Simulations performed using the Heart Simulator developed by Kelsey et al. (2002) based on Santamore and Burkhoff (1991). **c** Connecting points at the same time in the cardiac cycle illustrates the concept of time-varying elastance in the canine right ventricle (Maughan et al. 1979, Fig. 4)

popularized this framework and applied it to myocardial infarction (Suga et al. 1973; Suga and Sagawa 1974; Sunagawa et al. 1983).

When viewing a pressure-volume (PV) loop for the LV (Fig. 5), the events of the cardiac cycle are as follows: (i) the mitral valve opens at the lower left corner of the loop and blood flows from the left atrium into the relaxed LV (filling phase), generating a large increase in volume but relatively small change in pressure; (ii) at the lower right corner, contraction begins and pressure rises but volume does not change because both the mitral valve and aortic valve are closed (isovolumetric contraction); (iii) at the upper right corner, the LV pressure exceeds aortic pressure, forcing the aortic valve open and allowing the LV to eject blood into the aorta (ejection); (iv) at the upper left corner, the aortic valve closes and the LV pressure drops as the muscle in the wall relaxes (isovolumetric relaxation). The area within the loop represents the mechanical work performed by the LV in ejecting blood into the circulation.

3.1.1 Diastolic Function

The portion of the cardiac cycle during which the heart is passively filling (bottom portion of the PV loop) is called diastole. The main factors that control how much the heart fills during this phase include the material properties of the myocardium, the geometry of the LV, and the upstream pressure in the pulmonary veins and left atrium. At high heart rates or when the material properties of the myocardium are altered, the time available before the next contraction can also become an important determinant of filling. In theory, the resistance to blood flow through the open mitral valve could affect the rate of filling, but this is usually significant only in the setting of pathologic narrowing (stenosis) of the valve.

Suga and Sagawa (1974) and Sunagawa et al. (1983) performed many of their studies on isolated, blood-perfused canine hearts. This experimental preparation allowed them to separately vary factors that influence pump function and explore their impact individually. As one example, when they increased the upstream

pressure but held heart rate and the resistance to ejection through the aorta constant, the LV not only filled to higher volumes and pressures, but also ejected a larger volume of blood (stroke volume) with each contraction (Fig. 5a). This fundamental property of the heart is often called the Frank–Starling mechanism. At the level of individual myocytes, this property arises because increased diastolic stretch alters both the overlap between actin and myosin filaments and the binding of calcium to the myofilaments, increasing the active force generated by each cell during the subsequent contraction.

Another central experimental finding illustrated in Fig. 5a is that the lower right corners of PV loops with different filling pressures appear to lie along a single exponential curve. These points indicate pressures and volumes at the end of diastole when the heart muscle is fully relaxed, and the curve connecting them is termed the end-diastolic pressure-volume relationship (EDPVR). It is typically modeled using a simple equation that includes a volume intercept to account for the fact that even a completely unloaded, arrested LV has a nonzero cavity volume:

$$P_{\mathrm{ED}} = A\left\{\exp\left[B(V_{ED} - V_0)\right] - 1\right\}. \tag{5}$$

In part, the exponential shape of the diastolic pressure-volume relationship reflects the exponential stress–strain relationships measured in mechanical tests of the passive myocardium discussed in Sect. 1.2. However, one key point that may seem obvious to a mechanics audience has caused considerable confusion over the years among physicians and physiologists, because of the fact that many diseases alter the size and shape of the heart: both changes in material properties of the myocardium and changes in LV geometry will alter the EDPVR. One simple illustration of this concept is to imagine a pressurized, thin-walled elastic sphere. A force balance on one half of the sphere reveals that the force arising from the pressure pushing against the hemisphere must be balanced by the force associated with the stress in its wall; setting these two forces equal and simplifying yields an equation often termed Laplace's law. Thus,

$$Pr^2\pi = \sigma 2r\pi h \quad \rightarrow \quad \sigma = \frac{Pr}{2h}, \tag{6}$$

where h = wall thickness and r = radius. This equation shows clearly that at a given pressure the wall stress increases as radius increases and decreases as the wall thickens; thus, deformation will depend not only on material properties but also on geometry. While this simple equation is not appropriate for computing stresses in the thick-walled, elliptical LV, the same basic concepts apply to the heart: dilation (increased radius) shifts the EDPVR rightward (lower pressure at any volume), while wall thickening shifts the EDPVR leftward.

3.1.2 Systolic Function

When Sagawa and colleagues varied the resistance to ejection through the aorta in their isolated heart preparation and held heart rate and diastolic pressure constant, they saw that the LV ejected less blood against high resistance and more blood against low resistance, as expected (Fig. 5b). They also found that the upper left corners of the loops—indicating the pressure and volume at the end of systole for each beat—traced out a straight line. Although there are a few exceptions, this end-systolic pressure-volume relationship (ESPVR) is approximately linear in most animal models and under most loading conditions; e.g., inflating the LV to different diastolic volumes and then clamping the aorta to measure the maximum pressure generated during 'isovolumetric' beats yields basically the same relationship as connecting the upper left corners of normal, ejecting beats (Suga et al. 1973).

The linearity of the ESPVR is perhaps the single most remarkable finding in cardiac physiology: a complex structure composed of mechanically nonlinear and anisotropic materials generates a maximum pressure that is linearly proportional to cavity volume! The slope of the ESPVR, which Sagawa et al. (1988) termed the end-systolic elastance, E_{ES}, provides a very useful index of the 'contractility' of the heart. Drugs that increase calcium cycling and force of contraction in individual myocytes also increase E_{ES}, indicating that the heart can generate more isovolumetric pressure at a given volume or eject more blood against a given aortic resistance. The simple equation Sagawa et al. (1988) used to the describe the ESPVR is

$$P_{ES} = E_{ES}(V_{ES} - V_0), \tag{7}$$

where V_0 is a volume intercept at which no active pressure is generated by contraction.

Sagawa and his colleagues made one more discovery about the behavior of the LV that has proved invaluable in modeling heart function. When they varied filling pressures (preload) and resistance to ejection (afterload) to generate a range of PV loops, then connected PV points acquired at identical times after electrically stimulating the heart, they found that these isochronal points were connected by a family of lines (Fig. 5c). The slope of these lines increased as the LV contracted, reached a maximum at end systole (hence E_{ES} is also often called E_{max}), and then decreased again as the muscle in the LV relaxed. In other words, the LV can be reasonably modeled as a single chamber or compartment with a time-varying stiffness (Suga et al. 1973):

$$P(t) = E(t)(V(t) - V_0). \tag{8}$$

This is now known as the time-varying elastance model, and together with an experimentally measured curve for the time-varying slope $E(t)$, it provides a remarkably accurate prediction of PV loops for a given LV across a wide range of hemodynamic loading conditions. As we will see in the next section, the time-varying elastance framework also forms the basis for an influential analytical model of LV function in the setting of infarction.

3.2 Functional Impact of Myocardial Infarction

There are many different mechanisms by which a myocardial infarction can impair the pump function of the heart either directly or indirectly (Holmes et al. 2005); the related mechanics and physiology are discussed in detail in review articles by Holmes et al. (2005) and Richardson et al. (2015). This chapter focuses on the use of computational models in understanding and simulating these mechanisms and their effects on heart function; as an introduction, the mechanisms are reviewed briefly here. (i) The first mechanism by which infarction could impair function is particularly dramatic: if post-infarction necrosis weakens the infarct too much in the first few days before sufficient new collagen is deposited, the heart can rupture, leading to sudden death. (ii) A more common mechanism in the first few days after infarction is that the damaged region stretches passively as the rest of the heart contracts, reducing pressure generation and ejection from the LV and wasting mechanical energy; this mechanism and analytical models that capture it are discussed in detail in Sect. 3.2.1. (iii) Over time, as collagenous scar forms in the damaged region, systolic stretching becomes less problematic, but the stiff scar can limit LV filling during diastole; this mechanism is discussed in Sect. 3.2.2. (iv) A more subtle mechanism by which the infarct impairs LV function is that it is physically coupled to adjacent noninfarcted myocardium. Therefore, stretching, thinning, and outward bulging (dyskinesis) of the infarct can reduce thickening and inward motion in the borderzone, resulting in a region of functional depression that is bigger than the actual infarct. Anatomically detailed finite element models are needed to capture these three-dimensional interactions, as discussed in Sect. 4 of this chapter.

In addition to direct effects on function, myocardial infarction triggers a process of growth and remodeling that gradually alters function indirectly. (v) In the infarct region, collagen deposition can increase stiffness, affecting both systolic and diastolic function; in addition, gradual thinning of the infarct is common in most settings and acts to increase wall stress in the infarct and adjacent borderzone. (vi) In the surviving muscle, infarction triggers lengthening of individual myocytes with modest increases in cross-sectional area; at the chamber level, this is reflected in an increased cavity volume with relatively modest changes in wall thickness, a geometric change that increases wall stresses throughout the LV. Computational modeling of growth and remodeling following myocardial infarction is a young but exciting field, and is discussed in Sect. 5 of this chapter.

3.2.1 Systolic Function

The slope of the ESPVR provides a measure of the contractility of the heart. Therefore, it seems reasonable to expect that myocardial infarction will decrease this slope. Yet when Sunagawa et al. (1983) actually performed this experiment by ligating different coronary arteries in the isolated dog heart preparation, they found something unexpected: the slope of the ESPVR, E_{ES}, changed little, while the intercept, V_0,

increased in proportion to the size of the infarct! They also constructed a simple compartmental model that explained these apparently paradoxical results. The notation in the original paper is somewhat confusing, and has been modified here to improve clarity.

Sunagawa et al. (1983) knew that within a few seconds after coronary ligation, the ischemic region would stop contracting and begin passively stretching and recoiling with each beat. Accordingly, they modeled the LV as consisting of two compartments: a normally contracting compartment described by the usual time-varying elastance model, and a passive ischemic compartment where pressure and volume were related according to the EDPVR at all times. They assumed that the two compartments always operated at the same pressure but could contain different volumes, and computed the ESPVR for the two-compartment model using a weighted average of the end-systolic volumes that would be expected if the entire LV were contracting normally or the entire LV were ischemic. In the normal compartment

$$P_{ES} = E_{ES}(V_{ES} - V_0) \rightarrow V_{ES,n} = (1 - R)V_{ES} = (1 - R)\left(\frac{P_{ES}}{E_{ES}} + V_0\right), \quad (9)$$

and in the ischemic compartment

$$P_{ES} = A\left\{\exp\left[B(V_{ES} - V_0)\right] - 1\right\} \rightarrow V_{ES,i} = R\,V_{ES} = R\left[\frac{1}{B}\ln\left(\frac{P_{ES}}{A} + 1\right) + V_0\right], \quad (10)$$

yielding the overall ESPVR, i.e.

$$V_{ES} = V_{ES,n} + V_{ES,i} = (1 - R)\left(\frac{P_{ES}}{E_{ES}} + V_0\right) + R\left[\frac{1}{B}\ln\left(\frac{P_{ES}}{A} + 1\right) + V_0\right], \quad (11)$$

where R is the size of the ischemic region as a fraction of the LV. Figure 6 shows the predictions of this model for pressures and volumes typical of the experiments of Sunagawa et al. (1983), compared to original data from the paper. The key feature of the acutely infarcted heart that is captured by this simple model is the exponential nature of the EDPVR. Normally, diastolic pressures do not exceed 15–20 mmHg in the dog, but when the ischemic compartment is exposed to systolic pressures, it moves to a very steep portion of the EDPVR. At these high pressures, the slope of the EDPVR is very similar to the slope of the normal ESPVR, but the volumes are much larger. Thus, a weighted average of the behavior of the two compartments predicts a shift toward larger volumes (increased V_0) without much change in slope (unchanged E_{ES}).

The work of Sunagawa et al. (1983) is a wonderful example of the adage that a model should be as simple as possible, but not simpler. In this case, representing the complex, infarcted LV using two compartments—essentially two balloons

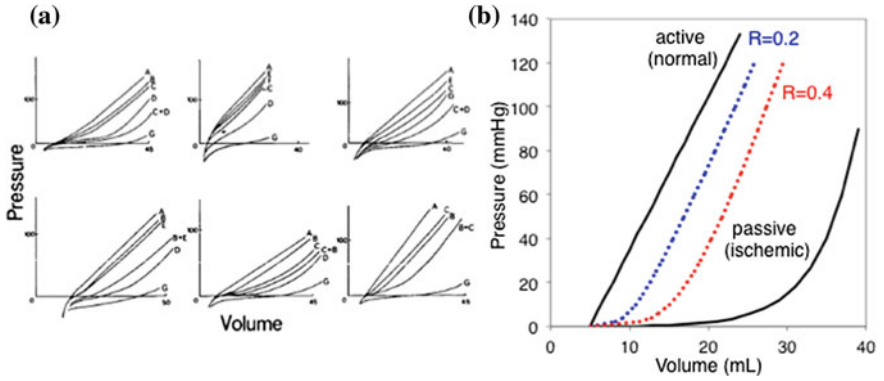

Fig. 6 **a** End-systolic pressure-volume relationships measured in six isolated dog hearts following coronary occlusions affecting different sized regions (Fig. 5 of Sunagawa et al. 1983, letters indicate which coronary branches were occluded). **b** Predictions of the two-compartment model of Sunagawa et al. (1983) (described in the text) for two different infarct sizes

connected by a straw—provides an accurate and useful analysis, as long as the exponential nature of the passive myocardium is incorporated. By contrast, simplifying the EDPVR by using a straight line—which is a fairly common and reasonable simplification in compartmental models operating in the range of diastolic pressures experienced by a normal heart—completely changes the behavior, resulting in an erroneous predicted decrease in E_{ES} during ischemia. Even a sophisticated finite element model would make similarly errant predictions if the ischemic region were assumed to be linearly elastic.

3.2.2 Diastolic Function

Three years before Sunagawa et al. (1983) published their compartmental model, Bogen et al. (1980) published a more complex analytical model that predicted similar pressure-volume behavior. They modeled the LV wall as a thin membrane with two sets of nonlinearly elastic material properties, simulating the myocardium as a softer, highly nonlinear material at end diastole, and a stiffer, less nonlinear material at end systole. Bogen et al. (1980) then assigned different material properties to one region of the simulated LV to represent infarcts at different stages of healing following infarction. Although representing the thick-walled LV as a thin-walled membrane did produce some unphysiologic predictions such as a sudden jump in stress at the infarct border, the model produced realistic diastolic and systolic pressure-volume behavior for both baseline and acute infarction cases.

More importantly, the model of Bogen et al. (1980) produced a fundamental insight about the impact of infarct stiffness on LV function that has since been verified in more sophisticated finite element models and experiments: stiffening the infarct improves systolic function by limiting bulging of the infarct, but impairs diastolic

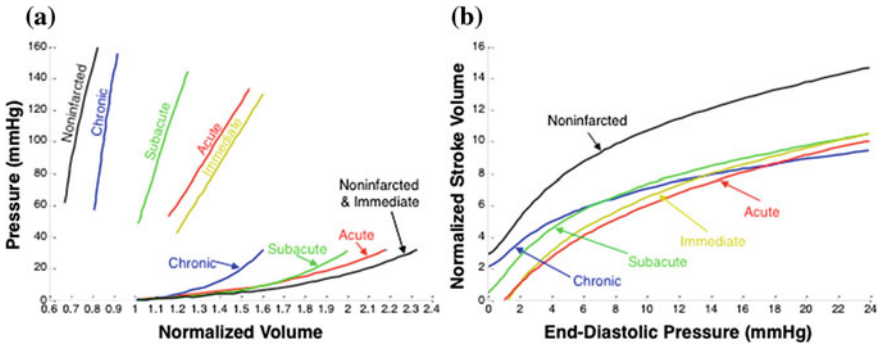

Fig. 7 **a** Predicted changes in end-systolic (ESPVR) and end-diastolic (EDPVR) pressure-volume relationships as the passive material properties of a large (41 % of LV) infarct region are increased to simulate different stages of infarct healing (replotted from Bogen et al. 1980); the ESPVR and EDPVR both shift left as infarct stiffness is increased. **b** Model ventricular function curves showing the net stroke volume pumped by the LV at different filling pressures in the presence of a moderate (25 %) infarct; stiffening the infarct yields little change in pump function at most filling pressures

function by restricting filling. As Bogen et al. (1980) increased the simulated stiffness of the infarct region in their model, the predicted ESPVR shifted to the left, reflecting an improved ability to eject blood against a given aortic resistance (Fig. 7a). At the same time, the predicted EDPVR shifted to the left, reflecting the fact that stiffening part of the LV reduces the overall chamber compliance. In order to understand the relative impact of these two effects, Bogen et al. (1980) plotted a ventricular function curve, showing the total stroke volume that would be expected at each filling pressure if afterload (resistance to ejection) were kept constant. Surprisingly, they found that the diastolic and systolic effects of infarct stiffening offset almost exactly, yielding no change in predicted pump function at most filling pressures across the entire range of infarct properties tested (Fig. 7b). This remarkable prediction has held up extremely well over more than three decades. More sophisticated finite element models (discussed in Sect. 4) have confirmed this prediction, and multiple experimental studies using surgical reinforcement or injection of polymers have shown that stiffening or reinforcing the infarct reduces diastolic and systolic volumes without changing stroke volume or cardiac output (Clarke et al. 2014; Richardson et al. 2015).

3.2.3 Coupling to the Circulation and Reflex Compensation

In vivo, the heart is coupled to the circulatory system, which regulates resistance to ejection from the ventricles during systole as well as the pressures driving filling during diastole. Therefore, understanding the physiology and mechanics of the heart in vivo often requires coupling models of the heart to models of the circulation. One of the most influential circulation models is the windkessel model, which incorporates the resistance of the peripheral arteries and capacitance of the aorta (Westerhof et al.

1969). This simple model explains how the arteries buffer pulses of flow from the LV during systole to provide continuous flow to the body. Building on the windkessel concept, Westerhof et al. (1969) developed more sophisticated circuit models of the circulation that better reflected the interaction between the heart and circulation on both the arterial and venous sides. Such lumped-parameter approaches form the basis for most mathematical models of the circulation. These lumped-parameter representations of the circulation are easily coupled not only to time-varying elastance models of heart mechanics but also to sophisticated finite element models (see, e.g., Kerckhoffs et al. 2007; Wall et al. 2012; Moyer et al. 2015).

The pressure in the systemic arteries is the driving force for blood flow through the body, and is determined by the balance between cardiac output and resistance to flow. The body senses changes to mean arterial pressure (MAP) through arterial baroreceptors and acts through compensatory reflexes to maintain MAP. During myocardial ischemia, reduced cardiac output should produce a fall in MAP; however, the circulation rapidly compensates by (i) increasing heart rate, (ii) increasing calcium cycling and the force the surviving myocardium can generate (contractility), and (iii) constricting peripheral blood vessels. Using a time-varying elastance model of the left and right ventricles coupled to a lumped-parameter model of the circulation, Burkhoff and Tyberg (1993) investigated the potential role of reflex hemodynamic compensation in generating pulmonary edema, one of the most serious consequences of acute left ventricular dysfunction. They found that even a large acute drop in left ventricular function caused relatively modest changes in pulmonary venous pressures if the parameters of the circulatory model were unaltered. Next, they simulated different reflex compensations that might be expected following a drop in LV function and found that only venoconstriction (a reduction in venous capacitance) substantially increased pulmonary venous pressures. Thus, they concluded that pulmonary edema was not a direct result of reduced left ventricular function, but rather a consequence of the reflex venoconstriction. Their work demonstrates both the power of mathematical modeling to provide new insights in cardiovascular physiology and the importance of the circulation in determining the consequences of changes in heart mechanics and function.

One of the most important long-term risks following myocardial infarction is the risk of developing heart failure. Here again, interaction of the heart, circulation, and hemodynamic reflexes likely plays an important role. Most standard post-infarction treatments primarily modulate the circulatory system or reflex compensations rather than the heart itself. Angiotensin converting enzyme (ACE) inhibitors, angiotensin receptor blockers, and a number of other drugs dilate arteries and veins. Beta blockers directly oppose reflex compensations, reducing both cardiac contractility and heart rate. Assessing the impact of even one of these drugs can be difficult as they often affect more than one cardiac or circulatory parameter. For example, Maurer et al. (2009) studied the effect of a common beta blocker, carvedilol, on patients with systolic heart failure. In patients who responded to carvedilol, Maurer et al. (2009) attributed 56 % of the increase in ejection fraction to heart rate reduction, 28 % to altered contractility, and 16 % to the reduction in total peripheral resistance using

multiple linear regression. In such situations, models can play an important role in estimating the relative importance of multiple simultaneous changes.

4 Finite Element Models of Ischemia and Infarction

Despite the success of the analytical models reviewed above in explaining global pressure-volume behavior in the infarcted heart, these simple models cannot accurately represent distributions of stresses and strains through the wall, mechanical interactions at the infarct border, or the effects of therapies such as polymer injection that perturb mechanics locally. Therefore, some questions related to the biomechanics of myocardial ischemia and infarction require anatomically realistic, detailed finite element models. Many investigators have developed and published finite element models of the heart over the past several decades; this review focuses on a few of these models selected for their historical value (Sect. 4.1) or as examples of particularly interesting applications of modeling to answer physiologic questions (Sect. 4.2) and design novel therapies (Sect. 4.3).

4.1 Early Models

One of the earliest modeling studies exploring interactions at the infarct border was published by Janz and Waldron (1978). They constructed an axisymmetric model of a rat LV based on geometry measured from a longitudinal (apex-base) slice through a fixed heart. They simulated a thinned, infarcted region at the apex of the model, and explored how stretches varied from the infarct into the adjacent normal myocardium during simulated passive inflation (diastole). When they simulated stiff chronic infarcts, circumferential stretch was low in the infarct and gradually increased with distance from the center of the infarct, reaching a normal (noninfarcted) value only in elements a substantial distance away from the infarct border. This simple result has potentially important physiologic consequences: because active force generation in cardiac muscle depends on diastolic sarcomere length (the Frank–Starling mechanism, discussed in Sect. 3.1.1), active contraction in normal myocardium near the infarct border could be impaired because diastolic prestretch is below normal.

Over the next two decades, most models of the ischemic or infarcted LV were conceptually similar, employing an axisymmetric elliptical geometry composed of a nonlinearly elastic passive material, then adding features such as active contraction or the presence of appropriately oriented fibers. Bovendeerd et al. (1996) published one of the last of this early class of models, integrating many of the most important features now common to modern models of the infarcted heart. Their model included muscle fibers with an orientation that varied through the wall, as described by Streeter and co-workers (Sect. 1.1), active stress generation in the direction of the fibers that depended on local diastolic prestretch, and a realistic infarct geometry

based on the perfusion territory of a branch of the left anterior descending coronary artery. They also simulated the full cardiac cycle rather than just end diastole and end systole, and—perhaps most importantly—compared their model predictions to hemodynamic data and epicardial surface strains measured in dogs during coronary occlusion. Bovendeerd et al. (1996) achieved an excellent match to experimentally measured fiber strains, then used their model to explore the impact of both transmural and non-transmural ischemia on regional work in the infarct borderzone.

4.2 Understanding Coupling to Adjacent Myocardium

Both models discussed in the previous section showed that the functional impact of a myocardial infarction could extend well beyond the infarct, into the surrounding myocardium near the infarct border. A number of groups subsequently used detailed finite element models of ischemia and infarction to explore this concept further. Mazhari and McCulloch (2000) and Mazhari et al. (2000) combined experiments and anatomically detailed finite element models of regional ischemia in the dog to ask whether the gradual transition from impaired to normal function across the infarct border implies a transition in local myocyte contractility. They found that they could reproduce measured distributions of fiber and crossfiber strain across the infarct border for a range of pressures and for different ischemic region locations even if they assumed a sudden step in contractility at the border of the ischemic region. In other words, mechanical interactions between the ischemic region and the surrounding myocardium are sufficient to create gradients in function that extend well beyond the infarct, even if the borderzone is composed of functionally normal myocytes.

Herz et al. (2005) applied similar models of regional ischemia to develop strategies for identifying and quantifying regional ischemia using three-dimensional echocardiography. Stress echocardiography is a common clinical test in which the heart is imaged using ultrasound both before and during elevation of cardiac energy consumption imposed by exercise or infusion of a drug such as dobutamine. Cardiologists typically evaluate the resulting images visually, looking for changes in inward motion or wall thickening (wall motion abnormality, WMA) that indicate compromised regional function due to a coronary stenosis that limits the increase in blood flow that would normally occur in response to stress. Herz et al. (2005) used finite element models to examine the relationship between the size of the simulated ischemic region and the size of the WMA as detected by various quantitative measures of endocardial motion. They found that with an appropriate choice of threshold, they could use quantitative wall motion measures to estimate the size of ischemic regions larger than about 10 % of the LV. However, small ischemic regions did not produce detectable wall motion abnormalities, because as the surrounding adjacent normal myocardium moved inward, it carried the ischemic region with it. Later, Herz et al. (2010) confirmed in animal experiments that most small ischemic regions induced no detectable WMA. Thus, whereas Mazhari and McCulloch (2000) and Mazhari

et al. (2000) showed that mechanical coupling to the ischemic region can cause dysfunction in surrounding myocardium, Herz et al. (2010) showed that coupling to the surrounding myocardium can also mask dysfunction in the ischemic region.

One final aspect of mechanical coupling that is of interest is the increase in wall stresses in the borderzone caused by the infarct. Myocytes generating higher stresses consume more oxygen and are energetically less efficient, so elevated wall stresses can be particularly disruptive in regions near an infarct where blood flow, systolic function, or both are already compromised. In addition, some investigators hypothesize that increased wall stress is a stimulus for growth and remodeling in myocardium, so elevated wall stress in the borderzone could contribute to the post-infarction remodeling that often leads to heart failure. Yet one of the central challenges of cardiac mechanics research is that it is virtually impossible to directly measure forces or stresses in the intact heart wall. Therefore, finite element models are an important tool for estimating wall stresses based on other, directly measurable quantities such as cavity pressure and regional strains. For example, Walker et al. (2005) constructed finite element models of the infarcted LV using geometry and regional strains measured by MRI in individual sheep with healed, large infarctions. They found that the presence of a healed infarct substantially increased stresses in the adjacent myocardium, particularly in the crossfiber direction. These studies set the stage for subsequent models of novel therapies intended to work partly or primarily by reducing wall stress following infarction.

4.3 Modeling and Designing Novel Therapies

One of the most exciting applications of finite element modeling of the heart is the design of novel post-infarction therapies. Drug and device therapies for heart disease are usually developed through trial-and-error. As one example, many years ago a series of studies tested the idea that lowering blood pressure might reduce remodeling of the heart following infarction. These studies culminated in a definitive clinical trial that showed that while lowering blood pressure did improve survival, one of the classes of antihypertensives—ACE inhibitors—conferred added benefit through an independent and previously unknown mechanism (Cohn et al. 1991). By contrast, current state-of-the-art finite element models are beginning to allow researchers to screen potential therapies computationally, testing a much wider range of ideas before beginning experimental trials of the most promising candidates.

Wall et al. (2006) published one of the earliest studies to harness the potential of model-based approaches in designing therapies. They used a finite element model of the infarcted sheep heart to simulate the effects of polymer injection into the infarct or adjacent borderzone, considering a range of potential polymer material properties, injection volumes, and injection patterns. They found that the volume of polymer injected was the most important determinant of how much the injection reduced wall stress, and that even relatively small volumes injected into the borderzone could substantially reduce elevated wall stresses by locally thickening the

heart wall. Importantly, some of the predicted effects were counterintuitive, such as the finding that stiffer polymers reduce wall stress when injected into the border, but actually exacerbate elevated borderzone stresses when injected into the infarct. Finally, some of the results confirmed predictions from earlier analytical models: injecting a stiff polymer into the infarct reduced both systolic and diastolic volumes, but produced no net improvement in the simulated ventricular function curve.

Fomovsky et al. (2011, 2012a) also published a series of studies illustrating the power of finite element models for designing post-infarction therapies. They returned to the original prediction by Bogen et al. (1980) that stiffening an infarct reduces diastolic and systolic volumes but does not improve overall pump function. Fomovsky et al. (2011) noted that prior analytical and finite element models of infarct stiffening typically treated the infarct as isotropic, whereas healing infarcts are often anisotropic (Sect. 2). Accordingly, they used a finite element model of the canine LV following a large anteroapical infarction to explore the functional impact of a wide range of both isotropic and anisotropic infarct material properties (Fig. 8a). They varied the ratio of coefficients controlling circumferential and longitudinal infarct stiffness in their Fung-type strain energy function from 60:1 to 1:60 and computed the predicted stroke volume at matched diastolic and systolic pressures for each choice of parameters. Surprisingly, they found that a scar that is much stiffer in the longitudinal direction than the circumferential direction—something that has never been observed in any animal model—provided the best predicted pump function (Fig. 8b). Unlike isotropic stiffening, selective stiffening in the longitudinal direction shifted the ESPVR to the left without altering diastolic function. Fomovsky et al. (2012a) then tested this prediction experimentally by selectively reinforcing acute canine infarcts in the longitudinal direction, and confirmed that anisotropic reinforcement provided the predicted improvement in pump function (Fig. 8c). This series of studies illustrates the promise of finite element modeling for identifying novel and potentially unexpected approaches by allowing exploration of a much larger parameter space than could ever be tested experimentally.

5 Models of Myocardial Infarct Healing

The studies by Wall et al. (2006) and Fomovsky et al. (2011, 2012a) reviewed in the previous section are excellent examples of the power of current models to predict the immediate effects of a novel therapy. Yet because the heart can grow and remodel in response to chemical or mechanical changes in its environment, predicting the short-term response is only half the battle. ACE inhibitors have modest acute effects on heart function, but improve survival over the long term by limiting growth and remodeling in the noninfarcted regions of the ventricle. Beta blockers—another class of drug given to most patients following infarction—actually depress heart function acutely, yet improve survival in the long term. The long-term effects of therapies on the healing infarct region are also important: e.g., steroids and other anti-inflammatory drugs were once tested as treatments to reduce infarct size, but ultimately abandoned

because they interfered with scar formation and increased the risk of dilation and rupture.

These examples illustrate the need to accurately predict not just short-term but also long-term effects of therapies on infarct healing and myocardial growth and remodeling. Predicting growth and remodeling is one of the newest and most exciting emerging areas within the field of biomechanics. This section focuses on early models of infarct healing, in keeping with the overall theme of the chapter. However, ongoing work on myocardial growth and remodeling in response to changes in hemodynamic loading will also prove important to developing new treatments for myocardial infarction, since the geometry and material properties of both the infarct region and the remaining undamaged myocardium ultimately determine long-term outcomes following myocardial infarction.

5.1 Inflammation and Cell–Cell Signaling

As discussed in Sect. 2, healing following myocardial infarction involves a series of different cell types that infiltrate the damaged region, remove damaged myocytes, and deposit scar tissue. The recruitment and activity of these cells are regulated in large part through a series of secreted factors called cytokines; therefore, modulating cell–cell signaling through cytokines is one potentially important approach to modulating infarct healing. Accordingly, Jin et al. (2011) developed a system of differential equations representing the infiltration and removal/death of key cell types as well as communication among these cell populations through some of the major known cytokines. Their model suggests that interactions among the different cell types involved in infarct healing can produce unexpected results in response

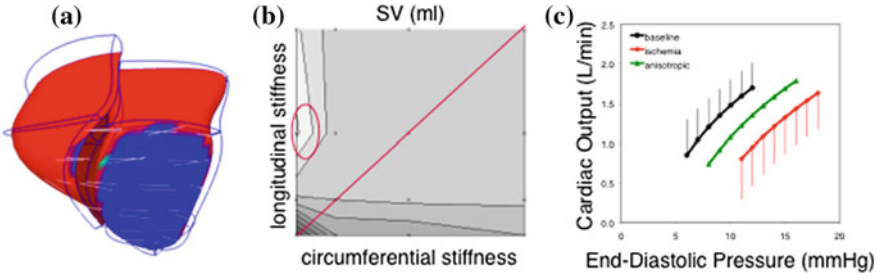

Fig. 8 **a** Finite element model of anteroapical infarction in the dog employed by Fomovsky et al. (2011). **b** Varying material parameters controlling circumferential and longitudinal infarct stiffness revealed that infarcts with high longitudinal and low circumferential stiffness (*circle*) had the best predicted pump function, while isotropic stiffening (*diagonal line*) had little effect across physiologically plausible values. **c** A subsequent experimental study confirmed that selective reinforcement in the longitudinal direction improved the cardiac output curve in infarcted canine hearts (Fomovsky et al. 2012a)

to potential therapies. As one example, increasing the level of TGF-β—which is generally considered a pro-fibrotic cytokine—actually reduced the predicted level of collagen deposition, by increasing the recruitment of macrophages that produce the collagen-degrading enzyme MMP-9.

5.2 Collagen Deposition and Alignment

Rouillard and Holmes (2012) developed an agent-based model (ABM) of infarct healing focused more narrowly on predicting the evolution of collagen alignment. The ABM tracked each fibroblast in the healing infarct as it migrated into the infarct, reorganized existing collagen, and deposited new collagen. The model considered two mechanisms by which fibroblast orientation could determine collagen orientation: fibroblasts deposited collagen fibers aligned with the cell, as has been shown in culture under some circumstances (Canty et al. 2006), and reoriented nearby collagen fibers, as has been demonstrated in collagen gels (Lee et al. 2008). At each time step, each cell selected an orientation and direction of motion from a probability distribution constructed by integrating multiple local factors known to influence fibroblast orientation in vitro: the prior direction (persistence), the spatial gradient of chemokines produced by inflammatory cells in the healing infarct (chemotaxis), the orientation of nearby collagen fibers (contact guidance), and the principal direction of stretch. The model also made a number of simplifications, such as attributing collagen degradation to fibroblasts rather than including other cell types that produce many of the collagen-degrading enzymes, and simulating the chemokine gradient as constant in time rather than varying over the course of the healing process.

Nevertheless, the ABM of Rouillard and Holmes (2012) was able to reproduce much of the data on scar structure reviewed under Sect. 2, including isotropic collagen orientation in ligation-induced rat infarcts and in cryoinfarcts stretching biaxially during healing, aligned collagen in rat cryoinfarcts stretching circumferentially during healing, and transmural gradients in collagen fiber orientation and alignment strength in healing pig infarcts, see Fig. 9. This last prediction was particularly interesting, because it shed new light on previously published but unexplained data. Experiments in healing pig infarcts revealed that during the first three weeks of healing the infarct experiences nearly uniaxial circumferential stretch; thus the direction of principal stretch conflicted with the orientation of the preexisting matrix in the epicardial (outer) and endocardial (inner) layers of the wall. The ABM predicted that these two conflicting cues would produce a relatively weak alignment signal in the inner and outer layers of the scar, and that collagen would gradually become more circumferential over time due to ongoing collagen turnover. By contrast, at the midwall the initial circumferential fiber orientation and the ongoing circumferential stretch would act synergistically, producing very high alignment in the circumferential direction. Remarkably, these predictions—achieved without tuning any of the parameters affecting cell and collagen orientation in the model—agreed very closely with published measurements (Fig. 9).

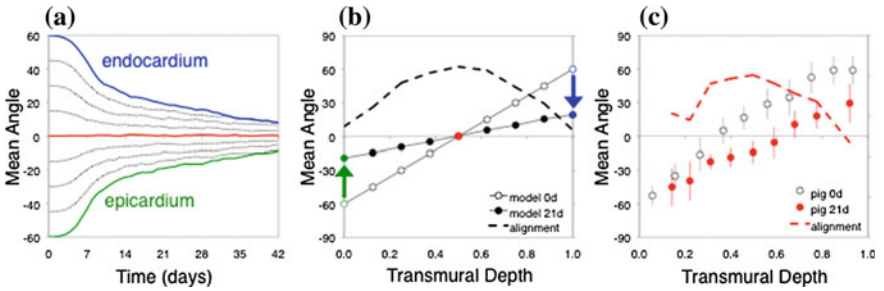

Fig. 9 Simulations of transmural variation in healing pig infarcts (data replotted from Rouillard and Holmes 2012): **a** Predicted mean angle in all transmural layers gradually converges toward 0° (circumferential), the direction of principal strain. **b** After 21 days of simulated healing, mean angles show some transmural variation, but less than in normal myocardium prior to infarction (0d); predicted alignment is strongest in the midwall, where preexisting matrix orientation and strain both promote circumferential alignment, and weakest at the epicardium and endocardium, where matrix and mechanical cues conflict. **c** Published data from Holmes et al. (1997) show a similar trend (data replotted from Holmes et al. 1997). *Note* alignment in panels **b** and **c** is plotted on an arbitrary scale

Models such as the one by Rouillard and Holmes (2012) represent a first step toward predicting the effects of therapeutic interventions on infarct healing. Their ABM could be used to predict an intervention with clear, known effects on one of the guidance cues (such as surgical reinforcement that alters stretch). However, the ABM is not currently able to predict the effects of drugs that alter intracellular signaling within fibroblasts or the cell–cell cytokine interactions modeled by Jin et al. (2011). Furthermore, changes in infarct healing may in turn influence scar mechanics, ventricular remodeling, systemic levels of hormones involved in reflex control of hemodynamics, etc. Ultimately, multi-scale models that represent intracellular signaling, cell–cell communication, scar formation, scar mechanics, ventricular mechanics and remodeling, and systemic hemodynamics and reflexes will be needed to fully predict the long-term effects of individual interventions.

6 Conclusions

Several themes are apparent from the experiments and models reviewed above. First, understanding the mechanics of myocardial infarction relies on high-quality data on the structure and mechanical properties of healing infarcts. Yet only a handful of studies have careful quantified these properties in multiaxial mechanical tests, and those studies produced conflicting data; clearly, more fundamental testing data are needed in order to understand the evolution of infarct mechanical properties and possible differences across species. The second broad theme is that computational models are essential in understanding the functional impact of myocardial infarction, because that impact depends not only on infarct mechanical properties but also

on interactions between the infarct and the surviving myocardium, and between the infarcted heart and the circulation. One clear, significant success of infarct biomechanics research to date is that current models are accurate enough to suggest novel, unexpected therapeutic approaches that work as predicted when tested experimentally. A critical future direction for infarct biomechanics is extending such models to incorporate the effects of drug and device therapies on wound healing in the infarct and on growth and remodeling in the rest of the heart. The final lesson apparent from the work reviewed here is that models do not always have to be complicated in order to provide useful insight. The analytical models of Sunagawa et al. (1983) and Bogen et al. (1980) captured essential features of the mechanics and physiology of the infarcted heart that remain relevant today, more than 30 years later.

References

Bell, R.M., Mocanu, M.M., Yellon, D.M.: Retrograde heart perfusion: the Langendorff technique of isolated heart perfusion. J. Mol. Cell Cardiol. **50**, 940–950 (2011)

Bogaert, J., Maes, A., Van de Werf, F., Bosmans, H., Herregods, M.C., Nuyts, J., Desmet, W., Mortelmans, L., Marchal, G., Rademakers, F.E.: Functional recovery of subepicardial myocardial tissue in transmural myocardial infarction after successful reperfusion: an important contribution to the improvement of regional and global left ventricular function. Circulation **99**, 36–43 (1999)

Bogen, D.K., Rabinowitz, S.A., Needleman, A., McMahon, T.A., Abelmann, W.H.: An analysis of the mechanical disadvantage of myocardial infarction in the canine left ventricle. Circ. Res. **47**, 728–741 (1980)

Bovendeerd, P.H., Arts, T., Delhaas, T., Huyghe, J.M., van Campen, D.H., Reneman, R.S.: Regional wall mechanics in the ischemic left ventricle: numerical modeling and dog experiments. Am. J. Physiol. **270**, H398–H410 (1996)

Buckberg, G., Hoffman, J.I.E., Mahajan, A., Saleh, S., Coghlan, C.: Cardiac mechanics revisited: the relationship of cardiac architecture to ventricular function. Circulation **118**, 2571–2587 (2008)

Burkhoff, D., Tyberg, J.V.: Why does pulmonary venous pressure rise after onset of LV dysfunction: a theoretical analysis. Am. J. Physiol. **265**, H1819–H1828 (1993)

Canty, E.G., Starborg, T., Lu, Y., Humphries, S.M., Holmes, D.F., Meadows, R.S., Huffman, A., O'Toole, E.T., Kadler, K.E.: Actin filaments are required for fibripositor-mediated collagen fibril alignment in tendon. J. Biol. Chem. **281**, 38592–38598 (2006)

Caulfield, J.B., Borg, T.K.: The collagen network of the heart. Lab. Invest. **40**, 364–372 (1979)

Clarke, S.A., Ghanta, R.K., Ailawadi, G., Holmes, J.W.: Cardiac restraint and support following myocardial infarction. In: Franz, T. (ed.) Cardiovascular and cardiac therapeutic devices, pp. 169–206. Springer, Berlin (2014)

Clarke, S.A., Goodman, N.C., Ailawadi, G., Holmes, J.W.: Effect of scar compaction on the therapeutic efficacy of anisotropic reinforcement following myocardial infarction in the dog. J. Cardiovasc. Transl. Res. **8**, 353–361 (2015)

Cohn, J.N., Johnson, G., Ziesche, S., Cobb, F., Francis, G., Tristani, F., Smith, R., Dunkman, W.B., Loeb, H., Wong, M., Bhat, G., Goldman, S., Fletcher, R.D., Doherty, J., Hughes, C.V., Carson, P., Cintron, G., Shabetai, R., Haakenson, C.: A comparison of enalapril with hydralazine-isosorbide dinitrate in the treatment of chronic congestive heart failure. N. Engl. J. Med. **325**, 303–310 (1991)

Connelly, C., Vogel, W.M., Hernandez, Y.M., Apstein, C.S.: Movement of necrotic wavefront after coronary artery occlusion in rabbit. Am. J. Physiol. **243**, H682–H690 (1982)

Costa, K.D., Takayama, Y., McCulloch, A.D., Covell, J.W.: Laminar fiber architecture and three-dimensional systolic mechanics in canine ventricular myocardium. Am. J. Physiol. **276**, H595–H607 (1999)

Costa, K.D., Holmes, J.W., McCulloch, A.D.: Modeling cardiac mechanical properties in three dimensions. Phil. Trans. R. Soc. Lond. A **359**, 1233–1250 (2001)

Criscione, J.C., Lorenzen-Schmidt, I., Humphrey, J.D., Hunter, W.C.: Mechanical contribution of endocardium during finite extension and torsion experiments on papillary muscles. Ann. Biomed. Eng. **27**, 123–130 (1999)

Demer, L.L., Yin, F.C.P.: Passive biaxial mechanical properties of isolated canine myocardium. J. Physiol. **339**, 615–630 (1983)

Dokos, S., Smaill, B.H., Young, A.A., LeGrice, I.J.: Shear properties of passive ventricular myocardium. Am. J. Physiol. Heart Circ. Physiol. **283**, H2650–H2659 (2002)

Fomovsky, G.M., Holmes, J.W.: Evolution of scar structure, mechanics, and ventricular function after myocardial infarction in the rat. Am. J. Physiol. Heart Circ. Physiol. **298**, H221–H228 (2010)

Fomovsky, G.M., Thomopoulos, S., Holmes, J.W.: Contribution of extracellular matrix to the mechanical properties of the heart. J. Mol. Cell Cardiol. **48**, 490–496 (2010)

Fomovsky, G.M., Macadangdang, J.R., Ailawadi, G., Holmes, J.W.: Model-based design of mechanical therapies for myocardial infarction. J. Cardiovasc. Transl. Res. **4**, 82–91 (2011)

Fomovsky, G.M., Clark, S.A., Parker, K.M., Ailawadi, G., Holmes, J.W.: Anisotropic reinforcement of acute anteroapical infarcts improves pump function. Circ. Heart Fail. **5**, 515–522 (2012a)

Fomovsky, G.M., Rouillard, A.D., Holmes, J.W.: Regional mechanics determine collagen fiber structure in healing myocardial infarcts. J. Mol. Cell Cardiol. **52**, 1083–1090 (2012b)

Frangogiannis, N.G.: The inflammatory response in myocardial injury, repair, and remodelling. Nat. Rev. Cardiol. **11**, 255–265 (2014)

Fujimoto, K.L., Tobita, K., Merryman, W.D., Guan, J., Momoi, N., Stolz, D.B., Sacks, M.S., Keller, B.B., Wagner, W.R.: An elastic, biodegradable cardiac patch induces contractile smooth muscle and improves cardiac remodeling and function in subacute myocardial infarction. J. Am. Coll. Cardiol. **49**, 2292–2300 (2007)

Guccione, J.M., McCulloch, A.D., Waldman, L.K.: Passive material properties of intact ventricular myocardium determined from a cylindrical model. J. Biomech. Eng. **113**, 42–55 (1991)

Gupta, K.B., Ratcliffe, M.B., Fallert, M.A., Edmunds Jr., L.H., Bogen, D.K.: Changes in passive mechanical stiffness of myocardial tissue with aneurysm formation. Circulation **89**, 2315–2326 (1994)

Herz, S.L., Ingrassia, C.M., Homma, S., Costa, K.D., Holmes, J.W.: Parameterization of left ventricular wall motion for detection of regional ischemia. Ann. Biomed. Eng. **33**, 912–919 (2005)

Herz, S.L., Hasegawa, T., Makaryus, A.N., Parker, K.M., Homma, S., Wang, J., Holmes, J.W.: Quantitative three-dimensional wall motion analysis predicts ischemic region size and location. Ann. Biomed. Eng. **38**, 1367–1376 (2010)

Ho, S.Y., Anderson, R.H., Sánchez-Quintana, D.: Atrial structure and fibres: morphologic bases of atrial conduction. Cardiovasc. Res. **54**, 325–336 (2002)

Holmes, J.W., Covell, J.W.: Collagen fiber orientation in myocardial scar tissue. Cardiovasc. Pathobiol. **1**, 15–22 (1996)

Holmes, J.W., Yamashita, H., Waldman, L.K., Covell, J.W.: Scar remodeling and transmural deformation after infarction in the pig. Circulation **90**, 411–420 (1994)

Holmes, J.W., Nuñez, J.A., Covell, J.W.: Functional implications of myocardial scar structure. Am. J. Physiol. Heart Circ. Physiol. **272**, H2123–H2130 (1997)

Holmes, J.W., Hünlich, M., Hasenfuss, G.: Energetics of the Frank–Starling effect in rabbit myocardium: economy and efficiency depend on muscle length. Am. J. Physiol. **283**, H324–H330 (2002)

Holmes, J.W., Borg, T.K., Covell, J.W.: Structure and mechanics of healing myocardial infarcts. Annu. Rev. Biomed. Eng. **27**, 223–253 (2005)

Holzapfel, G.A., Ogden, R.W.: Constitutive modelling of passive myocardium: a structurally based framework for material characterization. Phil. Trans. R. Soc. Lond. A **367**, 3445–3475 (2009)

Humphrey, J.D., Strumpf, R.K., Yin, F.C.P.: Determination of a constitutive relation for passive myocardium: I. A new functional form. J. Biomech. Eng. **112**, 333–339 (1990a)
Humphrey, J.D., Strumpf, R.K., Yin, F.C.P.: Determination of a constitutive relation for passive myocardium: II. Parameter estimation. J. Biomech. Eng. **112**, 340–346 (1990b)
Humphrey, J.D., Barazotto, R.L., Hunter, W.C.: Finite extension and torsion of papillary muscles: a theoretical framework. J. Biomech. **25**, 541–547 (1992)
Janz, R.F., Waldron, R.J.: Predicted effect of chronic apical aneurysms on the passive stiffness of the human left ventricle. Circ. Res. **42**, 255–263 (1978)
Jin, F.-Y., Han, H.-C., Berger, J., Dai, Q., Lindsey, M.L.: Combining experimental and mathematical modeling to reveal mechanisms of macrophage-dependent left ventricular remodeling. BMC Syst. Biol. **5**, 60 (2011)
Jugdutt, B.I., Amy, R.W.M.: Healing after myocardial infarction in the dog: changes in infarct hydroxyproline and topography. J. Am. Coll. Cardiol. **7**, 91–102 (1986)
Kelsey, R., Botello, M., Millard, B., Zimmerman, J.: An online heart simulator for augmenting first-year medical and dental education. Proc. AMIA Symp. 370–374 (2002)
Kerckhoffs, R.C.P., Neal, M.L., Gu, Q., Bassingthwaighte, J.B., Omens, J.H., McCulloch, A.D.: Coupling of a 3D finite element model of cardiac ventricular mechanics to lumped systems models of the systemic and pulmonic circulation. Ann. Biomed. Eng. **35**, 1–18 (2007)
Kidambi, A., Mather, A.N., Swoboda, P., Motwani, M., Fairbairn, T.A., Greenwood, J.P., Plein, S.: Relationship between myocardial edema and regional myocardial function after reperfused acute myocardial infarction: an MR imaging study. Radiology **267**, 701–708 (2013)
Kramer, C.M., Rogers, W.J., Theobald, T.M., Power, T.P., Geskin, G., Reichek, N.: Dissociation between changes in intramyocardial function and left ventricular volumes in the eight weeks after first anterior myocardial infarction. J. Am. Coll. Cardiol. **30**, 1625–1632 (1997)
Lee, J., Smith, N.P.: The multi-scale modelling of coronary blood flow. Ann. Biomed. Eng. **40**, 2399–2413 (2012)
Lee, E.J., Holmes, J.W., Costa, K.D.: Remodeling of engineered tissue anisotropy in response to altered loading conditions. Ann. Biomed. Eng. **36**, 1322–1334 (2008)
LeGrice, I.J., Smaill, B.H., Chai, L.Z., Edgar, S.G., Gavin, B., Hunter, P.J., Gavin, J.B.: Laminar structure of the heart: ventricular myocyte arrangement and connective tissue architecture in the dog. Am. J. Physiol. **269**, 571–582 (1995)
LeGrice, I.J., Hunter, P.J., Young, A., Smaill, B.H.: The architecture of the heart: a data-based model. Phil. Trans. R. Soc. Lond. A **359**, 1217–1232 (2001)
Lindsey, M.L., Zamilpa, R.: Temporal and spatial expression of matrix metalloproteinases and tissue inhibitors of metalloproteinases following myocardial infarction. Cardiovasc. Ther. **30**, 31–41 (2012)
Maughan, W.L., Shoukas, A.A., Sagawa, K., Weisfeldt, M.L.: Instantaneous pressure-volume relationship of the canine right ventricle. Circ. Res. **44**, 309–15 (1979)
Maurer, M.S., Sackner-Bernstein, J.D., El-Khoury Rumbarger, L., Yushak, M., King, D.L., Burkhoff, D.: Mechanisms underlying improvements in ejection fraction with carvedilol in heart failure. Circ. Heart Fail. **2**, 189–196 (2009)
May-Newman, K., Omens, J.H., Pavelec, R.S., McCulloch, A.D.: Three-dimensional transmural mechanical interaction between the coronary vasculature and passive myocardium in the dog. Circ. Res. **74**, 1166–1178 (1994)
Mazhari, R., McCulloch, A.D.: Integrative models for understanding the structural basis of regional mechanical dysfunction in ischemic myocardium. Ann. Biomed. Eng. **28**, 979–990 (2000)
Mazhari, R., Omens, J.H., Covell, J.W., McCulloch, A.D.: Structural basis of regional dysfunction in acutely ischemic myocardium. Cardiovasc. Res. **47**, 284–293 (2000)
McCallum, J.B.: On the muscular architecture and growth of the ventricles of the heart. Johns Hopkins Hospital Reports. **9**, 307–335 (1900)
McCormick, R.J., Musch, T.I., Bergman, B.C., Thomas, D.P.: Regional differences in LV collagen accumulation and mature cross-linking after myocardial infarction in rats. Am. J. Physiol. **266**, H354–H359 (1994)

McCulloch, A.D., Smaill, B.H., Hunter, P.J.: Left ventricular epicardial deformation in isolated arrested dog heart. Am. J. Physiol. **252**, H233–H241 (1987)
McCulloch, A.D., Smaill, B.H., Hunter, P.J.: Regional left ventricular epicardial deformation in the passive dog heart. Circ. Res. **64**, 721–733 (1989)
Morita, M., Eckert, C.E., Matsuzaki, K., Noma, M., Ryan, L.P., Burdick, J.A., Jackson, B.M., Gorman, J.H., Sacks, M.S., Gorman, R.C.: Modification of infarct material properties limits adverse ventricular remodeling. Ann. Thorac Surg. **92**, 617–624 (2011)
Moyer, C.B., Norton, P.T., Ferguson, J.D., Holmes, J.W.: Changes in global and regional mechanics due to atrial fibrillation: insights from a coupled finite-element and circulation model. Ann. Biomed. Eng. **43**, 1600–1613 (2015)
Nash, M.P., Hunter, P.J.: Computational mechanics of the heart. J. Elasticity **61**, 113–141 (2001)
Novak, V.P., Yin, F.C.P., Humphrey, J.D.: Regional mechanical properties of passive myocardium. J. Biomech. Eng. **27**, 403–412 (1994)
Omens, J.H., Miller, T.R., Covell, J.W.: Relationship between passive tissue strain and collagen uncoiling during healing of infarcted myocardium. Cardiovasc. Res. **33**, 351–358 (1997)
Richardson, W.J., Clark, S.A., Holmes, J.W.: Physiological implications of myocardial scar structure. Compr. Physiol. **5**, 1877–1909 (2015)
Rivlin, R.S., Saunders, D.W.: Large elastic deformations of isotropic materials. VII. Experiments on the deformation of rubber. Phil. Trans. R. Soc. Lond. A **243**, 251–288 (1951)
Rouillard, A.D., Holmes, J.W.: Mechanical regulation of fibroblast migration and collagen remodelling in healing myocardial infarcts. J. Physiol. **590**, 4585–4602 (2012)
Rushmer, R.F., Crystal, D.K., Wagner, C.: The functional anatomy of ventricular contraction. Circ. Res. **1**, 162–170 (1953)
Sagawa, K., Maughan, L., Suga, H., Sunagawa, K.: Cardiac contraction and the pressure-volume relationship. Oxford University Press, New York (1988)
Santamore, W.P., Burkhoff, D.: Hemodynamic consequences of ventricular interaction as assessed by model analysis. Am. J. Physiol. **260**, H146–57 (1991)
Schmid, H., Nash, M.P., Young, A.A., Hunter, P.J.: Myocardial material parameter estimation - a comparative study for simple shear. J. Biomech. Eng. **128**, 742–750 (2006)
Schmid, H., O'Callaghan, P., Nash, M.P., Lin, W., LeGrice, I.J., Smaill, B.H., Young, A.A., Hunter, P.J.: Myocardial material parameter estimation: a non-homogeneous finite element study from simple shear tests. Biomech. Model. Mechanobiol. **7**, 161–173 (2008)
Sommer, G., Haspinger, D.C., Andrä, M., Sacherer, M., Viertler, C., Regitnig, P., Holzapfel, G.A.: Quantification of shear deformations and corresponding stresses in the biaxially tested human myocardium. Ann. Biomed. Eng. **43**, 2334–2348 (2015)
Streeter, D.D.: Gross morphology and fiber geometry of the heart. In: Berne, R.M. (ed.) Handbook of physiology: the cardiovascular system, pp. 61–112. Williams & Wilkins, Baltimore (1979)
Streeter, D.D., Hanna, W.T.: Engineering mechanics for successive states in canine left ventricular myocardium. I. Cavity and wall geometry. Circ. Res. **33**, 639–655 (1973a)
Streeter, D.D., Hanna, W.T.: Engineering mechanics for successive states in canine left ventricular myocardium. II. Fiber angle and sarcomere length. Circ. Res. **33**, 656–664 (1973b)
Suga, H., Sagawa, K.: Instantaneous pressure-volume relationships and their ratio in the excised, supported canine left ventricle. Circ. Res. **35**, 117–126 (1974)
Suga, H., Sagawa, K., Shoukas, A.A.: Load independence of the instantaneous pressure-volume ratio of the canine left ventricle and effects of epinephrine and heart rate on the ratio. Circ. Res. **32**, 314–322 (1973)
Sunagawa, K., Maughan, W.L., Sagawa, K.: Effect of regional ischemia on the left ventricular end-systolic pressure-volume relationship of isolated canine hearts. Circ. Res. **52**, 170–178 (1983)
Tennant, R., Wiggers, C.J.: The effect of coronary occlusion on myocardial contraction. Am. J. Physiol. **112**, 351–361 (1935)
Theroux, P., Ross, J., Franklin, D., Covell, J.W., Bloor, C.M., Sasayama, S.: Regional myocardial function and dimensions early and late after myocardial infarction in the unanesthetized dog. Circ. Res. **40**, 158–165 (1977)

Torrent-Guasp, F.: On morphology and cardiac function. 4th communication. Rev. Española Cardiol. **20**, 2–13 (1967)
Tyberg, J.V., Forrester, J.S., Wyatt, H.L., Goldner, S.J., Parmley, W.W., Swan, H.J.: An analysis of segmental ischemic dysfunction utilizing the pressure-length loop. Circulation **49**, 748–754 (1974)
Usyk, T., Mazhari, R., McCulloch, A.D.: Effect of laminar orthotropic myofiber architecture on regional stress and strain in the canine left ventricle. J. Elasticity **61**, 143–164 (2000)
Villareal, F.J., Lew, W.Y., Waldman, L.K., Covell, J.W.: Transmural myocardial deformation in the ischemic canine left ventricle. Circ. Res. **68**, 368–381 (1991)
Vivaldi, M.T., Eyre, D.R., Kloner, R.A., Schoen, F.J.: Effects of methylprednisolone on collagen biosynthesis in healing acute myocardial infarction. Am. J. Cardiol. **60**, 424–425 (1987)
Walker, J.C., Ratcliffe, M.B., Zhang, P., Wallace, A.W., Fata, B., Hsu, E.W., Saloner, D., Guccione, J.M.: MRI-based finite-element analysis of left ventricular aneurysm. Am. J. Physiol. Heart Circ. Physiol. **289**, H692–H700 (2005)
Wall, S.T., Walker, J.C., Healy, K.E., Ratcliffe, M.B., Guccione, J.M.: Theoretical impact of the injection of material into the myocardium: a finite element model simulation. Circulation **114**, 2627–2635 (2006)
Wall, S.T., Guccione, J.M., Ratcliffe, M.B., Sundnes, J.S.: Electromechanical feedback with reduced cellular connectivity alters electrical activity in an infarct injured left ventricle: a finite element model study. Am. J. Physiol. Heart Circ. Physiol. **302**, H206–H214 (2012)
West, J.B.: Best and Taylor's physiological basis of medical practice, 11th edn. Williams and Wilkins, Baltimore (1985)
Westerhof, N., Bosman, F., De Vries, C.J., Noordergraaf, A.: Analog studies of the human systemic arterial tree. J. Biomech. **2**, 121–143 (1969)
White, H.D., Chew, D.P.: Acute myocardial infarction. Lancet **372**, 570–584 (2008)
Whittaker, P., Boughner, D.R., Kloner, R.A.: Analysis of healing after myocardial infarction using polarized light microscopy. Am. J. Pathol. **134**, 879–893 (1989)
Yin, F.C.P., Strumpf, R.K., Chew, P.H., Zeger, S.L.: Quantification of the mechanical properties of noncontracting canine myocardium under simultaneous biaxial loading. J. Biomech. **20**, 577–589 (1987)
Zhao, J., Butters, T.D., Zhang, H., Pullan, A.J., LeGrice, I.J., Sands, G.B., Smaill, B.H.: An image-based model of atrial muscular architecture: effects of structural anisotropy on electrical activation. Circ. Arrhythm. Electrophysiol. **5**, 361–370 (2012)
Zimmerman, S.D., Thomas, D.P., Velleman, S.G., Li, X., Hansen, T.R., McCormick, R.J.: Time course of collagen and decorin changes in rat cardiac and skeletal muscle post-MI. Am. J. Physiol. Heart Circ. Physiol. **281**, H1816–H1822 (2001)